Differential Membrane Binding and Seeding of Distinct α-Synuclein Fibrillar Polymorphs

Amulya Nidhi Shrivastava, Luc Bousset, Marianne Renner, Virginie Redeker, Jimmy Savistchenko, Antoine Triller, Ronald Melki

Differential Membrane Binding and Seeding of Distinct α-Synuclein fibrillar polymorphs

Short Title: Functional properties of distinct α-Synuclein fibrillar polymorphs

Amulya Nidhi Shrivastava[1,4,*], Luc Bousset[1], Marianne Renner[2], Virginie Redeker[1], Jimmy Savistchenko[1], Antoine Triller[3,*] and Ronald Melki[1,*]

1 CEA, Institut François Jacob (MIRcen) and CNRS, Laboratory of Neurodegenerative Diseases, 18 Route du Panorama, 92265, Fontenay-aux-Roses, France.
2 INSERM, UMR- S 839 Institut du Fer à Moulin (IFM), Sorbonne Université, Paris, France.
3 École Normale Supérieure, Institut de Biologie de l'ENS (IBENS), INSERM, CNRS, PSL Research University, 46 Rue d'Ulm, 75005 Paris, France
4 Current affiliation: UCB Biopharma SRL, 1420, Braine Braine l'Alleud, Belgium

Correspondance:
*** Ronald Melki (ronald.melki@cnrs.fr)**
*** Antoine Triller (triller@biologie.ens.fr)**
*** Amulya Nidhi Shrivastava (amulya.nidhi@gmail.com)**

Abstract (138 words)

The aggregation of the protein α-Synuclein (α-Syn) leads to different synucleinopathies. We recently showed that structurally distinct fibrillar α-Synuclein polymorphs trigger either Parkinson's Disease or Multiple System Atrophy hallmarks *in vivo*. Here, we establish structural-molecular basis for these observations. We show that distinct fibrillar α-Syn polymorphs bind to and cluster differentially at the plasma membrane in both primary neuronal cultures and organotypic hippocampal slice cultures from wild-type mice. We demonstrate a polymorph-dependent and concentration-dependent seeding. We show a polymorph-dependent differential synaptic re-distribution of α3-Na^+/K^+-ATPase, GluA2-AMPA and GluN2B-NMDA receptors but not GluA1-AMPA and mGluR5 receptors. We also demonstrate polymorph-dependent alteration in neuronal network activity upon seeded aggregation of α-Syn. Our findings bring new insight into how distinct α-Syn polymorphs differentially bind to and seed monomeric α-Syn aggregation within neurons, thus affecting neuronal homeostasis through the redistribution of synaptic proteins.

Keywords: α-Synuclein fibrillar polymorphs, protein-protein interaction, membrane protein clustering, seeding, synaptic function

Introduction

Synucleinopathies are a class of neurodegenerative diseases that have in common the aggregation of the protein α-Synuclein (α-Syn). They comprise Parkinson's disease (PD) without or with dementia, Dementia with Lewy bodies (DLB), Multiple System Atrophy (MSA), Gaucher disease (Wong & Krainc, 2017; Melki, 2015). It has been proposed that different synucleinopathies are the consequence of the aggregation of α-Syn into high molecular weight assemblies that possess distinct intrinsic structures (Melki, 2017, 2015). Indeed, α-Syn chameleon property yields multiple conformations allowing the formation of fibrillar assemblies with distinct structures and surfaces that dictate their growth and clearance propensities. Experimental evidence for polymorphs-pathology interdependence came from recent works (Peelaerts *et al*, 2015; Bousset *et al*, 2013; Guo *et al*, 2013; Prusiner *et al*, 2015) where different α-Syn fibrillar polymorphs injection in rodent brains yielded phenotypes characteristic of PD and MSA.

The distinct intrinsic architectures different α-Syn polymorphs possess is due to the different amino acid stretches involved in their amyloid core (Bousset *et al*, 2013). Given that different amino acid stretches are involved in distinct α-Syn polymorphs amyloid core (Verasdonck *et al*, 2016; Bousset *et al*, 2013), those they expose at their surfaces also differ (Melki, 2018). The tip and the side surfaces of pathogenic α-Syn fibrillar assemblies possess have to be considered separately. The growing ends define the rate at which they elongate by recruitment of monomeric α-Syn in conformations that can establish highly complementary interactions. The amino acid stretches exposed on the sides of distinct α-Syn polymorphs define what membranous components, in particular plasma membrane proteins, they can interact with. Recent studies reported the interaction of exogenous fibrillar α-Syn with extracellularly exposed membrane proteins (Shrivastava *et al*, 2015; Holmes *et al*, 2013). The presence of those protein partners and their abundance on neuronal plasma membrane define the tropism of distinct α-Syn polymorphs toward cell populations within the central nervous system.

After binding and take up of fibrillar α-Syn, seeding occurs (Brundin *et al*, 2010). This is accompanied in cell cultures and in vivo by post-translational modifications ranging from proteolytic cleavages to phosphorylation, ubiquitination etc. of newly aggregated endogenous α-Syn. Efficient seeding of neuronal α-Syn by exogenous fibrils has been demonstrated

(Volpicelli-Daley *et al*, 2011). Organotypic slice cultures represent a powerful alternative to primary neuronal cultures as they allow assessing seeding and propagation of infectious proteins in a context where neuronal circuits are maintained partially intact. Organotypic slices have been indeed widely used to study prion pathology (Goniotaki *et al*, 2017; Falsig *et al*, 2012; Sonati *et al*, 2013). Here we show that five distinct fibrillar α-Syn polymorphs (Fibrils, Ribbons, Fibrils-91, Fibrils-65 and Fibrils-110) bind to and cluster differentially at the plasma membrane in both primary neuronal cultures and organotypic hippocampal slice cultures from wild-type mice. We demonstrate a polymorph-dependent and concentration-dependent seeding. We prove that a fibrillar polymorph's initial binding and clustering to the plasma membrane is tightly linked to subsequent pS129-α-Syn aggregates accumulation. We also report a fibrillar polymorph-dependent differential synaptic re-distribution of α3-subunit of Sodium/Potassium-ATPase (α3-NKA), GluA2 subunit containing α-amino-3-hydroxy-5-methyl-4-isoxazolepropionic acid (GluA2-AMPA) receptors and GluN2B-subunit containing N-methyl-D-aspartate (GluN2B-NMDA) receptors. We also demonstrate fibrillar polymorphs-dependent alteration in neuronal network activity upon seeded aggregation of α-Syn. Altogether, our findings suggest that distinct α-Syn fibrillar polymorphs differentially affect neuronal homeostasis.

Results

Differential α-Syn fibrillar polymorphs binding and clustering on primary neuronal cultures

We previously demonstrated the ability of monomeric α-Syn to assemble into fibrillar polymorphs that differ through the conformation the protein adopts within the fibrils and the packing of α-Syn molecules within the fibrils under different experimental conditions (Makky *et al*, 2016; Bousset *et al*, 2013; Verasdonck *et al*, 2016). The resulting pure polymorphs differ in their shape on transmission electron micrographs (**Figure 1A**, top row). The polymorphs were fragmented so that they have the same average length (**Figure 1A**, bottom row, **1B**). They possess distinct limited proteolytic patterns, with the exception of Fibrils and Fibrils-65, because they expose differently proteinase K cleavage sites (**Figure 1C**). These proteolytic patterns can be compared to "fingerprints" reflecting the different conformations α-Syn molecules adopt within distinct fibrillar polymorphs. They also exhibit distinct physical and pathogenic properties (Peelaerts *et al*, 2015; Makky *et al*, 2016).

To determine to what extent the intrinsic structure of fibrillar α-Syn polymorphs affect binding to neurons, we exposed primary neurons at DIV 21 (Days *In Vitro*) to identical concentrations of ATTO-550 labeled Fibrils, Ribbons, Fibrils-91, Fibrils-65 and Fibrils-110 (50nM) (Makky *et al*, 2016) for 5min or 60min. At these time points, most of the fibrillar α-Syn remain bound to the plasma membrane (Shrivastava *et al*, 2015). The cultures were next immunolabeled for Homer to identify excitatory synapses along the dendrites (**Figure 2A**). The images reveal striking differences. Fibrils-91 bound to neurons with a much better efficiency as compared to the polymorph Fibrils (3 fold- difference; **Figure 2A**, Row 1 and 3). In contrast, Fibrils-65 and Fibrils-110 bound to neurons with much less efficiency than α-Syn polymorph Fibrils. Ribbons bound to neurons with an efficiency significantly higher than that of Fibrils but lower than that of Fibrils-91. The "fluorescence of α-Syn cluster", indicative of the size of the cluster, and the "number of α-Syn clusters per μm^2", characteristic of density, were quantified (**Figure 2B** and **C,** respectively). The size of α-Syn Ribbons clusters was larger than that of the fibrillar polymorph Fibrils (**Figure 2B**), whereas both exhibited similar density (**Figure 2C**). In contrast, the size and density of α-Syn Fibrils-91 clusters were significantly larger than those of α-Syn polymorph Fibrils. Both the binding efficiency and the density of the cluster Fibrils-65 and Fibrils-110 formed on neurons were significantly lower than those of the polymorph Fibrils.

In the primary hippocampal neuronal cultures, 80-85% synapses are excitatory. We therefore assessed the partial co-localization/apposition of α-Syn fibrillar polymorphs with the excitatory synapse marker, Homer. Nearly 15-25% of the clusters of the fibrillar α-Syn polymorphs that bound efficiently to neurons (e.g. Fibrils, Ribbons and Fibrils-91) co-localized with excitatory synapses (**Figure 2D**), independent from the exposure time (5min or 60min). The figure was smaller, 0-12% co-localization with Homer for the two fibrillar polymorphs (Fibrils-65 and 110) that bound significantly less efficiently to neurons. This is in line with our previous study where we reported that α-Syn Fibrils form clusters at both synaptic and extra-synaptic and also on axon and dendrites (**Supplementary Figure 1**) (Shrivastava *et al*, 2017, 2015). Our observations undoubtedly demonstrate that distinct α-Syn fibrillar polymorphs bind to and cluster on neuron plasma membrane to different extents. We therefore conclude from these observations that the amino acid stretches exposed at the surfaces of distinct pathogenic α-Syn fibrillar assemblies define the efficiency with which they bind to neuronal plasma membranes.

Nanoscopic properties of fibrillar α-Syn fibrillar polymorph clusters on neuronal membrane

Confocal imaging and threshold-based analysis (**Figure 2**) are biased towards larger clusters and provide no information about diffused single-molecules (non-clustered) and molecules forming nanoclusters. These limitations are solved by the use of super-resolution imaging. We therefore performed Stochastic Optical Reconstruction Microscopy (STORM) on fixed neurons exposed to the different fibrillar α-Syn polymorphs (50nM, 60min) labeled with ATTO-647N dye, as in a previous study (Shrivastava *et al*, 2015). Representative rendered images of the fibrillar polymorphs Fibrils, Fibrils-91 and Ribbons.with a pointing accuracy of 10nm are shown (**Figure 3A**, upper row). Density-based spatial clustering of applications with noise (DBSCAN), a point-detection based clustering algorithm, was employed to confine analysis to authentic clusters (Ester *et al*, 1996; Malkusch & Heilemann, 2016) (**Figure 3A**, bottom row). The density of the polymorphs Fibrils and Ribbons bound to neurons (single molecule detections per μm^2) (**Figure 3B**) were similar but smaller (1.5 fold lower) than that observed for Fibrils-91 (**Figure 3B**). Albeit this, as much as 90% of all single molecule detections events for all three α-Syn fibrillar polymorphs were localized within the clusters identified by DBSCAN (**Figure 3C**). These observations clearly indicate that α-Syn fibrillar polymorphs have a high propensity to form clusters on the plane of the plasma membrane. Cumulative distribution of area of all clusters (n=Fibrils: 7681, Ribbons: 4600, Fibrils-91: 8672) show a wide distribution. The distribution reveals significant differences between the clusters the three fibrillar polymorphs form (**Figure 3D**). Compared to Fibrils, the polymorph Ribbons populates small sized clusters (area < 5000 nm^2). The polymorph Fibrils-91, populates very large clusters (>200000 nm^2) that are neither observed for Fibrils nor Ribbons.

We further performed Single Particle Tracking (SPT) of α-Syn fibrillar polymorphs on the plasma membrane of live neurons using STORM (SPT-STORM). For this pre-formed α-Syn fibrillar polymorphs were labeled using Photoactivable Janelia Farm 647 Dye (Grimm *et al*, 2016). This powerful imaging approach allowed us to track the dynamic behavior of thousands of α-Syn single fibrillar particles on neuron membranes and quantify their dynamics prior to clusters formation. The measurements were performed within 10-min after exposure of neurons to α-Syn-polymorphs (50nM) to track specifically membrane bound assemblies. Representative images (**Figure 3E**) show single particle trajectories of α-Syn

Fibrils-91 at two magnifications. By using variational Bayesian treatment of hidden Markov models (Persson *et al*, 2013) that combine information from thousands of short single-particle trajectories, 3-diffusive states of α-Syn were extracted with confidence. Particles in state 1 represents fast diffusing, most likely, one fibril; particles in state 2 exhibit intermediate diffusion velocity, they diffuse as small complexes; particles in state 3 are characterized by slow-diffusion velocity, they represent clustered α-Syn fibrillar assemblies (**Figure 3F-G**). Comparison of the diffusion coefficients indicate that the polymorphs Fibrils and Fibrils-91 but not Ribbons diffuse identically in all three states. This indicate that the polymorphs Ribbons and Fibrils/Fibrils-91 interact differentially with membrane components. Single molecules can exchange between diffusive states (**Figure 3F**), therefore we quantified the dwell-time of a single molecule in a given diffusive state. All α-Syn-polymorphs exhibit higher dwell-time in state 3 i.e. in clustered state (**Figure 3H**) compared to non-clustered states (state 1 and 2). This validates the observation that α-Syn has a high propensity to form clusters (**Figure 3B**). Interestingly, in diffusive state 3, Ribbons exhibit lower dwell-time values compared to Fibrils/Fibrils-91 (**Figure 3H**). This strongly suggests that the clusters Ribbons form are less stable than those Fibrils/Fibrils-91 yield. The occupancy time (i.e. the time spent by single particles in each diffusive state is plotted (**Figure 3I**). The three polymorphs spend less time (20%) in state 1 (as single particle) compared to state 2/3 (in a larger complex), indicating cluster formation following diffusion.

Time-dependent endocytosis of fibrillar assemblies

Following binding to the membrane, fibrillar α-Syn polymorphs are internalized (Flavin *et al*, 2017; Abounit *et al*, 2016). We quantified the rate of initial endocytosis of distinct fibrillar α-Syn polymorphs as this is key for subsequent seeding within neuronal cells. Primary mature neurons at DIV 21 (Days *In Vitro*) were exposed to fibrillar α-Syn polymorphs for 1h (50nM, dual labeled with biotin and ATTO488) (**Figure 4A**), followed by removal of unbound assemblies. Cells were fixed immediately (0h condition) or after 4h/8h of exposure. While total (surface + endocytosed) α-Syn polymorphs were detected based on ATTO488 fluorescence, those at cell surface were detected using streptavidin-550, that binds to biotin. ATTO488-spots that did not co-localize with Streptavidin-550 spots depicted endocytosed fibrillar α-Syn. As shown in the representative example (**Figure 4B**), a small proportion of fibrillar α-Syn polymorphs were endocytosed (green only spots) within this time frame. Quantification showed a small but significant, time-dependent increase in the number of

internalized fibrillar α-Syn spots for all three polymorphs (**Figure 4C**). Notably for all fibrillar polymorphs, 5-15% spots were found endocytosed, the remaining fraction was localized at the plasma membrane. This contrasts with fibrillar α-Syn polymorphs differential binding and suggests that the rate of endocytosis of various α-Syn polymorphs of similar length is independent from their intrinsic structures in agreement with previous observations (Flavin *et al*, 2017).

Differential seeding by fibrillar α-Syn polymorphs in primary neuronal cultures

To determine whether the differential binding of distinct fibrillar α-Syn polymorphs reflects in their seeding propensity, we assessed quantitatively the aggregation of endogenous α-Syn using mature primary neuronal cultures. Hippocampal neurons at DIV 14, when synapses and spines (Ivenshitz & Segal, 2010) are formed, were exposed to the three fibrillar α-Syn polymorphs that bind best to neurons, e.g. Fibrils, Ribbons and Fibrils-91 for 15min (250nM). At DIV 21, cells were fixed and immunolabeled for pS129-α-Syn using 81A antibody (**Figure 5A**). Few processes (nearly 3-5 on an 18-mm cover-slip with 100,000 cells plated) were pS129-α-Syn positive after exposure of neurons to the polymorphs Fibrils (**Figure 5B-C**). The number of pS129-α-Syn positive processes was significantly larger upon exposure of neurons to the polymorph Ribbons and even larger upon exposure to the polymorph Fibrils-91 (**Figure 5B-C**). The pS129-α-Syn we detected is of endogenous nature as similar results were obtained with exogenous fibrillar polymorphs made of an α-Syn version (α-Syn S129A) that cannot be phosphorylated on Serine residue 129 (**Supplementary Figure 2**). As expected, pS129-α-Syn immunoreactivities were located within axons (**Figure 5D**), where endogenous α-Syn is expressed (Unni *et al*, 2010). The autophagosome marker p62/Sequestosome-1 co-localized with pS129-α-Syn bundles within the cell body (**Figure 5E**) but not with those in the axons (**Figure 5E**, arrows). pS129-α-Syn bundles within the cell body also co-localized with ubiquitin (**Figure 5F**). To determine whether seeding affects the integrity of neurons in primary cultures, neurons were stained with anti-Homer antibodies and the density of synapses was quantified. A slight reduction in Homer-positive synapses was observed in neurons where endogenous α-Syn was seeded by Fibrils-91 (**Supplementary Figure 3A**).

1%-Sarkosyl extract was prepared from seeded neurons and analyzed on 12% SDS-PAGE gel without a stacking layer. Western-blot analysis revealed pS129-α-Syn immunoreactivity for

Ribbons and Fibrils-91 polymorphs (**Figure 5G**, left). Mice specific α-Syn detected monomeric (all conditions) as well as aggregated α-Syn (Ribbons and Fibrils-91 conditions) (**Figure 5G**, middle). Surprisingly, the immunoreactivity for Fibrils-91 was not higher than that of Ribbons as anticipated. This could be due to differential turnover of pS129-α-Syn aggregates seeded by Fibrils, Fibrils-91 and Ribbons. We conclude from these observations that α-Syn fibrillar polymorphs binding to neurons is key for seeding endogenous α-Syn. Indeed, the fibrillar polymorph that bound the best within 1h (**Figure 2**) seeded most after 1 week (**Figure 5**).

Seeded pS129-α-Syn aggregates are composed of multiple elongated intertwined structures

We performed STORM imaging to visualize seeded pS129-α-Syn at higher resolution to determine whether they exhibit different macromolecular characteristics. Aggregated axonal pS129-α-Syn exhibited multiple microscopic elongated structures irrespective of the fibrillar polymorphs the neurons were exposed to (**Figure 6A-C**). The thickness of the elongated structures was within the range 30-40nm. We next assessed the time course of these elongated structures formation using the polymorph Fibrils-91, that yields the largest amount of pathology. Aggregated axonal pS129-α-Syn formation was imaged by STORM after exposure of primary neurons to fibrillar polymorphs for 2, 3 and 6 days (**Figure 6D**). The elongated structures appear as early as 2 days' post-exposure. They are fewer in number at 2 (**Figure 6D**, top panel) than 3 (**Figure 6D,** middle panel) and 6 (**Figure 6D**, bottom panel) days post-exposure. Quantification confirms that the number of pS129-α-Syn molecules (detection events) within the aggregates (**Figure 6E**) and the area occupied by aggregates (**Figure 6F**) increases from day 2 to 6. STORM imaging also revealed a time-dependent thickening of those elongated structures with the appearance of bundles (**Figure 6D,** bottom row).

Differential α-Syn fibrillar polymorphs binding and seeding in organotypic slice cultures

To determine whether fibrillar α-Syn polymorphs binding to neurons and seeding *in vivo* mirrors the observations we report using primary neuronal culture, we developed an *ex vivo* organotypic hippocampal slices model. Slices, maintained for 2-weeks after plating were exposed for 15min to the fibrillar polymorphs Fibrils, Ribbons and Fibrils-91 labeled with

ATTO-550 (0.75µM). The different fibrillar α-Syn polymorphs bound to all the available surface of organotypic slices (**Figure 7A**). As for primary neuronal cultures, the polymorph Fibrils bound the least while the polymorph Fibrils-91 bound the most (**Figure 7A-B**). Seeding of endogenous α-Syn by the different fibrillar polymorphs was next assessed. The slices were fixed 4, 7 or 14 days' post-exposure to exogenous fibrillar α-Syn polymorphs (**Figure 7C-E**) and aggregated α-Syn was detected using pS129-α-Syn immunolabeling with the mouse monoclonal antibody 81A (**Figure 7**, green). Processes immunopositive for pS129-α-Syn were visible as early as 4 days after exposure to the polymorph Fibrils 91, not to the other fibrillar polymorphs (**Figure 7D-E**). At day 7, few pS129-α-Syn positive processes were detected in slices exposed to the polymorphs Fibrils and Ribbons (**Figure 7D-E**). By day 14, slices exposed to Ribbons exhibited a larger number of pS129-α-Syn positive processes than those exposed to Fibrils albeit less than those exposed to Fibrils-91 (**Figure 7D-E**). No hippocampal region specificity was observed. As for the primary neuronal cultures, pS129-α-Syn aggregates are made from the endogenous α-Syn, as similar results were obtained with exogenous fibrillar polymorphs made of an α-Syn version (α-Syn S129A) that cannot be phosphorylated on Serine residue 129 (**Supplementary Figure 4**). The residual fluorescence of exogenous fibrillar α-Syn polymorphs were also assessed on day 4, 7 and 14 (**Figure 7F**). A time-dependent decrease, demonstrating clearance/degradation of exogenous fibrillar α-Syn polymorphs was observed.

Loosely packed aggregated bundles of endogenous pS129-α-Syn (**Figure 7G-H**, green) were observed in neurons cell body (**Figure 7G**, grey) either frequently or occasionally upon exposure of the slices to the fibrillar polymorphs Fibrils-91 or Ribbons, respectively. The extent of pS129-α-Syn aggregation was very low (**Figure 7E**) in slices exposed to the polymorph Fibrils, and no aggregated bundles were seen in the experimental time frame. These structures stained positive for autophagosome marker p62/Sequestosome-1 (**Figure 7H**, red). Notably, p62 only co-localized with cytosolic bundled aggregates, but not individual processes (**Figure 7H**, arrows) as observed in primary cultures (**Figure 5E**).

The dependence of seeding on the concentration of exogenous fibrillar α-Syn polymorphs was next assessed. For all three fibrillar polymorphs, a significant increase in the amount of pS129-α-Syn labeling was observed upon increasing seeds concentration by two-fold (**Figure**

7I). The increase in the median values was 100.5%, 621.2%, and 73.4%, for the fibrillar polymorphs Fibrils, Ribbons and Fibrils-91, respectively (**Figure 7J**).

To determine whether seeding affects neuronal integrity within the organotypic slices, the slices were stained with anti-Homer antibodies and the density of synapses was quantified after seeding. No reduction in Homer-positive synapses was observed (**Supplementary Figure 3B**). Additionally, no observable difference in neuronal labeling was observed 1-week after seeding with the different fibrillar polymorphs (**Supplementary Figure 5**). We conclude from these observations that distinct fibrillar α-Syn polymorphs bind and trigger the aggregation of endogenous α-Syn to different extents *ex vivo*. We further conclude that they do so in a concentration-dependent manner within the concentration range we explored.

We also assessed the localization of p129-α-Syn relative to oligodendrocytes, and the impact of microglia depletion from the organotypic slices on p129-α-Syn deposits. We found no p129-α-Syn deposits in Olig2 positive cells for slices exposed to Fibrils/Fibrils-91 polymorphs. For Ribbons, we did observe occasional p129-α-Syn reactivity within Olig2-positive oligodendrocytes (**Supplementary Figure 6**). As the exposed surfaces of organotypic slices are known to be enriched in microglia we depleted completely those cells by colony-stimulating factor 1 receptor (CSF1R) inhibitor, PLX3397 (Elmore *et al*, 2014). This did not alter p129-α-Syn immunoreactivity demonstrating that microglia do not affect seeding in neurons in our setup (**Supplementary Figure 7**).

Differential re-distribution of synaptic α3-NKA/GluA2-AMPA/GluN2B-NMDA in primary neurons exposed to α-Syn fibrillar polymorphs.

We next assessed the distribution of key synaptic components in seeded neurons by immunohistochemistry. Exposure was performed on DIV 14 for 15min and the cells were fixed on DIV 21 as above. No synaptic morphological changes were observed within the experimental time frame we used in agreement with previous observations (Shrivastava *et al*, 2015). Dual-detection was performed for α3-subunit of Na^+/K^+-ATPase (α3-NKA) (**Figure 8A-B**), GluA1-subunit of AMPA receptors (**Figure 8F-G**), GluA2-subunit of AMPA receptors (**Figure 8C-D**), GluN2B-subunit of NMDA receptors (**Figure 8E-F**), or metabotropic glutamate receptor 5 (mGluR5) (**Figure 8H-I**) along with Homer or PSD95 to identify excitatory synapses. Increased α3-NKA, GluA2-AMPA and GluN2B-NMDA but not

GluA1-AMPA receptor or mGluR5 at synapses was observed for neurons exposed to α-Syn fibrillar polymorph Fibrils (**Figure 8**). Neurons exposed to α-Syn polymorph Fibrils-91 exhibited increased synaptic clustering of α3-NKA but not GluA2-AMPA GluN2B-NMDA, GluA1-AMPA receptors or mGluR5 (**Figure 8**). In contrast, exposure of neurons to α-Syn fibrillar polymorph Ribbons did not lead to a change in the synaptic distribution of any of the proteins or receptors we examined (**Figure 9**). Our measurements demonstrate that α-Syn fibrillar polymorphs Fibrils and Fibrils-91 but not Ribbons alter excitatory synaptic receptors composition. We conclude from these observations that distinct α-Syn fibrillar polymorphs differentially redistribute key synaptic components in seeded neurons likely due to homeostatic dysregulation.

Alteration in network activity in primary neurons seeded with fibrillar α-Syn polymorphs

We next assessed the impact of fibrillar α-Syn polymorphs seeding on spontaneous neuronal activity using Multi-Electrode Array (MEA) recordings. Primary neurons were grown on 120 electrodes MEA plates and their activity was sampled at 10 kHz. To account for the inherent differences in network development between cultures, we recorded spontaneous neuronal activity on DIV 14 (2h before exposure to α-Syn fibrillar polymorphs) and on DIV 21 (1-week after exposure). Raster plots show the network activity in each MEA where each row represents the spiking activity around individual electrode (**Figure 9A-D**). As evident from the raster plots, the most significant decrease in neuronal spiking rate was observed in Fibrils-seeded neurons (**Figure 9B, 9E**). Neurons seeded with the polymorphs Ribbons and Fibrils-91 exhibit no or weak reduction in neuronal activity (**Figure 9**). This observation together with the finding that neurons exposed to the polymorph Fibrils exhibit the lowest pS129-α-Syn load (**Figure 5C**) and the strongest re-distribution of synaptic receptor (**Figure 8B, D and F**) suggest that neuronal network activity is most affected by the polymorph Fibrils.

Discussion

We and others previously showed that mega-Dalton fibrillar α-Syn assemblies propagate from cell to cell (Rey *et al*, 2016; Hansen *et al*, 2011; Luk *et al*, 2012; Freundt *et al*, 2012; Peelaerts *et al*, 2015; Brahic *et al*, 2016). This is consistent with the hypothesis made by Braak for the spread of a pathogen within the central nervous system via neuroanatomical connections in Parkinson's disease (Braak *et al*, 2003). We also established that exogenous fibrillar assemblies made of wild type α-Syn with distinct structural properties trigger pathological phenotypes characteristic of PD and MSA and imprint their structural characteristics to the monomeric α-Syn they recruit (Bousset *et al*, 2013; Peelaerts *et al*, 2015). This suggests a structure-pathology relationship. We demonstrate here that distinct WT α-Syn fibrillar polymorphs bind to neurons with different efficiencies. We show that the binding, take-up and seeding of distinct exogenous α-Syn fibrillar polymorphs alters synaptic NMDA/AMPA/α3-NKA distribution to different extents. We bring evidence for a tight relationship between binding and seeding efficiencies in *in vitro* and an *ex vivo* model of synucleinopathy. Indeed, we show that distinct exogenous α-Syn fibrillar polymorphs trigger the aggregation of endogenous monomeric α-Syn to different extents. This indicates that the binding of exogenous fibrillar α-Syn polymorphs to neurons is key for take-up and amplification by seeding. Our findings further establish the function of the plasma membrane as a chemical reactor favoring molecular interactions and the formation of protein clusters by restricting α-Syn fibrillar polymorphs diffusion space from 3D to 2D (Shrivastava *et al*, 2017).

Differential fibrillar α-Syn polymorphs binding and clustering in primary and organotypic slice cultures

Intra-cerebral injection of exogenous α-Syn assemblies is widely used to document their prion-like propagation and the accumulation of pS129-α-Syn (Mougenot *et al*, 2012; Hansen *et al*, 2011; Peelaerts *et al*, 2015; Guo *et al*, 2013; Luk *et al*, 2012). This experimental approach is nonetheless unsuitable to assess cellular mechanistic processes occurring within short timeframes (hours to days) following the interaction of exogenous α-Syn assemblies with a naïve neuron. Indeed, detectable levels of pathological pS129-α-Syn deposits appear only 2-3 months post-injection, after spine loss begins (Blumenstock *et al*, 2017). Primary neuronal culture models represent an alternative to *in vivo* studies (Volpicelli-Daley *et al*, 2011). However, most existing protocols are based on the continuous exposure of 5-7-days

old neurons, that lack mature synapses (Ichikawa *et al*, 1993), to exogenous α-Syn assemblies. We therefore developed a robust model based on the use of 14-21 days old primary neurons and backed it up with 14-28 days-old organotypic slice cultures, where neuronal circuitry is maintained, to assess over minutes to 2 weeks the binding and seeding propensities of exogenous fibrillar α-Syn polymorphs and the consequences of these events. We chose hippocampal neurons despite the fact that the striatum and substantia nigra are affected most in vivo by Lewy pathology. This choice is justified by the fact that seeded aggregation of α-Syn in hippocampal neurons has been well documented (Volpicelli-Daley *et al*, 2011) and our recent finding that seeding in hippocampal neurons is more efficient than in cortical and striatal counterparts (Courte et al., in revision).

The distinct intrinsic structures fibrillar α-Syn polymorphs exhibit are due to the different conformations monomeric α-Syn adopts within the fibrillar particles. This reflects in their shapes, morphology, proteolytic patterns, physical properties (Verasdonck *et al*, 2016; Bousset *et al*, 2013; Makky *et al*, 2016) and is expected to define their interactomes as distinct polymorphs must expose different amino acid stretches at their surfaces. Recent studies reported the interaction of exogenous fibrillar α-Syn with extracellularly exposed membrane proteins (Shrivastava *et al*, 2015; Holmes *et al*, 2013). The recent cryo-electron microscopy structure for the polymorph Fibrils reveals indeed what amino acid stretches and side chains are exposed to the solvent (Guerrero-Ferreira *et al*, 2019). The amino acid stretches that define the interactome of the polymorph Fibrils we use here differ from those reported to be exposed to the solvent in fibrillar polymorphs generated by others (Li *et al*, 2018a; Rodriguez *et al*, 2015; Tuttle *et al*, 2016; Li *et al*, 2018b). Despite the fact that the amino acid stretches the distinct fibrillar polymorphs we use here, with one exception, are unknown, we know they differ as the fibrillar polymorphs amyloid core are unlike (Bousset *et al*, 2013; Verasdonck *et al*, 2016). We demonstrate here that α-Syn polymorphs surfaces indeed define their functional properties. They bind differentially to neuronal plasma membranes, cluster and alter synaptic α3-NKA, NMDA and AMPA receptors distribution to different extents, minutes to hours after binding and 7 days later on when uptake and seeding of endogenous α-Syn has occurred.

Differential fibrillar α-Syn polymorphs seeding

Strain-dependent differential seeding is known for various amyloidogenic proteins such as scrapie-prions, α-Syn, tau and amyloid-beta (Aguzzi *et al*, 2007; Kaufman *et al*, 2016; Guo *et al*, 2013; Peelaerts *et al*, 2015). We demonstrate here a relationship between binding and seeding. The polymorphs that bind best, Fibrils-91, seed to the highest extent. Thus, the differential binding of distinct fibrillar α-Syn polymorphs appears key for their take-up, escape from the endo-lysosomal compartments (Flavin *et al*, 2017) and seeding within the cytosol of recipient neurons. As the distinct fibrillar α-Syn polymorphs were fragmented in order to have an average length of 40-50 nm compatible with endocytosis, differential take-up cannot account for the different seeding propensities we report. As the different polymorphs have different structures, as demonstrated by solid state NMR measurements (Bousset *et al*, 2013; Verasdonck *et al*, 2016), they expose different amino acid stretches on their surfaces (Melki, 2018). Once taken up, distinct fibrillar polymorphs grow at very different rates as their different ends recruit monomeric α-Syn at rates highly dependent on the abundance of the conformation that can establish highly complementary interactions with their ends. Furthermore, as distinct α-Syn polymorphs expose on their sides different amino acid stretches, they resist clearance to different extents and interact differentially with partner molecules ranging from proteins to lipids. Taken together, the differential binding, growth rates and resistance of distinct fibrillar α-Syn polymorphs account for their differential accumulation within neurons.

Interestingly, super-resolution imaging revealed that the endogenous, seeded, α-Syn aggregates have elongated structures (30-50nm width) that bundle over time into structures resembling Lewy neurites. Whether these structures are polymorph-specific and possess defined structures, remains unclear and cryo-electron microscopy may allow determining whether, in a manner similar to PolyQ inclusions, they consist of fibrils interacting with cellular endomembranes originating from the endoplasmic reticulum (Bäuerlein *et al*, 2017).

Functional consequences of the differential interaction of fibrillar α-Syn polymorphs with neuronal membrane components

Synapses are dynamic and they re-model in an activity and signaling dependent manner (Choquet & Triller, 2013). Differential re-distribution of synaptic membrane proteins, but not scaffolds (homer, PSD) was observed in α-Syn polymorphs seeded neurons. This suggest that the different polymorphs trigger different molecular signaling pathways. Increased synaptic

clustering of α3-NKA was observed upon exposure of neurons to the polymorphs Fibrils and Fibrils-91 but not Ribbons. The redistribution of this pump is deleterious as it prevents the extrusion of sodium ion out of neurons (Shrivastava *et al*, 2015, 2019). Therefore, it is likely that the polymorphs Fibrils and Fibrils-91 impact a neuron's capacity to extrude sodium ions by forming aberrant clusters. Such aberrant clustering α3-NKA create regions within the plasma membrane with reduced local densities of α3-NKA (Shrivastava *et al*, 2018).

We previously showed that α-Syn polymorph Fibrils do not interact directly with AMPA and NMDA receptors (Shrivastava *et al*, 2015). Nonetheless, this polymorph triggered increased synaptic accumulation of GluA2-subunit containing AMPA and GluN2B-subunit containing NMDA receptors. Thus, the re-distribution of AMPA/NMDA is most likely due to homeostatic dysregulation following perturbation of several signalling pathways (Choquet & Triller, 2013). The polymorph Fibrils-91 also triggered an increase in synaptic accumulation of GluA2-AMPA but not GluN2B-NMDA receptors. Fibrils and Fibrils-91-mediated glutamate receptors re-distribution at synapses should trigger an enhanced activity-evoked calcium influx and possibly synaptic impairment. No redistribution of those major synaptic components was observed upon exposure of neurons to the polymorph Ribbons. This suggests that the fibrillar polymorph Ribbons either affects a yet unknown pathway or target other neuronal cells (Peelaerts *et al*, 2015). Several pathogenic assemblies: α-Syn (Ferreira *et al*, 2017), amyloid-β (Renner *et al*, 2010; Shrivastava *et al*, 2013; Um *et al*, 2013) and scrapie prions (Goniotaki *et al*, 2017) have been shown to interact with mGluR5 via PrP^c. None of the fibrillar α-Syn polymorphs we used altered mGluR5 distribution.

Neurons where α-Syn aggregation was seeded by Fibrils, but not Ribbons and Fibrils-91 exhibited gross alteration in neuronal network activity without measurable alterations in synapses density. Neurons exposed to the polymorph Fibrils exhibit the lowest pS129-α-Syn load and the strongest re-distribution of synaptic receptor. Altogether, our findings suggest that neuronal network activity is most affected by the re-distribution of synaptic receptors without measurable alterations in synapses density upon exposure of naïve neurons to pathogenic α-Syn assemblies. This unexpected finding may indicate that synaptic dysfunction and network imbalance precedes the appearance of pathology. Contrarily, neurons where α-Syn aggregation was seeded with Fibrils-91 displayed extensive pathology but no alteration in network activity. The latter neurons likely compensate for the loss of activity over time, but

fail to prevent cytosolic aggregation. These aggregates are potential source of “traffic-jams” within the cell where different cytosolic proteins and organelles get trapped.

Altogether our results suggest a sequential deleterious scenario where the binding of distinct α-Syn fibrillar polymorphs to neuron plasma leads to differential redistribution of essential membrane proteins, synaptic remodeling and impaired neuronal activity. Following take-up, distinct α-Syn fibrillar polymorphs further trigger noxious changes with the differential seeded aggregation of endogenous α-Syn and the impact this has on normal cytosolic trafficking and mitochondrial function (Gribaudo et al., 2019; Valdinocci et al., 2019; Ordonez et al., 2018). This is of particular interest in a context where recent reports bring solid evidence for the existence of α-Syn polymorphs in the brain of patients who developed distinct synucleinopathies (Strohäker *et al*, 2019) and for their capacity to selectively target brain regions and cells types from the central nervous system (Lau *et al*, 2019; Rey *et al*., 2019). Our results together with recent reports using patients-derived pathogenic α-Syn highlight the importance of targeting α-Syn aggregates prion-like propagation in therapeutic approaches to synucleinopathies. As for de novo generated α-Syn fibrillar polymorphs, the future assessment of patients-derived pathogenic α-Syn aggregates, amplified ex vivo or not, ability to differentially redistribute neuron membrane proteins, remodel synapses and seed the aggregation of α-Syn in neurons may bring novel insights into synucleinopathies.

Overall, we demonstrate here that α-Syn polymorphs surfaces define their binding and seeding propensity with subsequent differential redistribution of partner proteins at synapses and consequences on neuronal network activity. These findings are consistent with the view that distinct synucleinopathies may result from the changes in neuronal membrane and cytosolic protein homeostasis different α-Syn polymorphs trigger.

Material and Methods

Generation, labeling and characterization of fibrillar α-syn polymorphs

The expression and purification of human wild-type (WT) α-Syn was performed as previously described (Ghee *et al*, 2005). A variant human α-Syn where Serine 129 residue was changed to Alanine (S129A α-Syn) was generated by site directed mutagenesis. This variant cannot be phosphorylated in neurons on S129, the main phosphorylation site for α-Syn. S129A α-Syn was purified exactly as wild-type (WT) α-Syn. WT α-Syn or S129A α-Syn was incubated in buffer A to obtain the fibrillar polymorph "Fibrils" (50 mM Tris–HCl, pH 7.5, 150 mM KCl), in buffer B for "Ribbons" (5 mM Tris–HCl, pH 7.5), in buffer C for "Fibrils-65" (20mM MES pH6,5, 150mM NaCl) and in buffer D for "Fibrils-91" (20mM KPO4 pH9.1), at 37°C under continuous shaking in an Eppendorf Thermomixer set at 600 r.p.m for 4-7 days (Bousset *et al*, 2013; Makky *et al*, 2016). A truncated human α-Syn spanning residues 1-110 was generated by introducing 2 stop codons after residue 110 by site directed mutagenesis. This variant was purified exactly as full-length α-Syn and was assembled into fibrillar structures "Fibrils-110" in buffer A (50 mM Tris–HCl, pH 7.5, 150 mM KCl). The fibrillar α-Syn polymorphs were centrifuged twice at 15,000 *g* for 10 min and re-suspended twice in PBS at 1,446g/L. All preformed assemblies were labeled with ATTO-488 NHS-ester, ATTO-550 NHS-ester or ATTO-647N NHS-ester (Atto-Tec Gmbh # AD 488-3, AD 550-35 and AD 647N-35, respectively) fluorophore following the manufacturer's instructions and/or biotin using EZ-link Sulfo-NHS-Biotin (sulfosuccinimidobiotin, Perbio Science, UK) using a protein:dye/tag ratio of 1:2. The labeling reactions were arrested by addition of 1mM Tris pH 7.5. The unreacted fluorophore was removed by a final cycle of two centrifugations at 15,000 *g* for 10 min and resuspensions of the pellets in PBS. Mass-spectrometry was used to quantify the number of incorporated ATTO or biotin molecules per α-Syn monomer within the fibrillar assemblies as previously described (Shrivastava *et al*, 2019, 2015). This labelling protocol typically yields ≤ 1 ATTO or biotin molecules incorporated per α-Syn monomer on average (**Supplementary Figure 8**). The quality control of human recombinant monomeric WT or S129A α-Syn and the fibrillar polymorphs they generate and that of α-Syn 1-110 were carried out as previously described (Bousset *et al*, 2013; Makky *et al*, 2016). The fibrillar polymorphs were fragmented by sonication for 20 min in 2-ml Eppendorf tubes in a Vial Tweeter powered by an ultrasonic processor UIS250v (250 W, 2.4 kHz; Hielscher Ultrasonic, Teltow, Germany) to generate fibrillar particles with an average size 42-52 nm that are suitable for endocytosis.

For transmission electron microscopy, the assemblies were adsorbed on 200 mesh carbon coated electron microscopy grids and imaged after negative staining with 1% uranyl acetate before and after fragmentation using a Jeol 1400 electron microscope. For fibrillar polymorphs finger print analysis, we used degradation by proteinase K. Aliquots of fibrillar assemblies were removed before or after addition of proteinase K (3.8µg ml^{-1}), denatured in boiling Laemmli buffer for 5 minutes at 90°C, subjected to SDS-PAGE on 12% polyacrylamide gels and stained by Coomassie coloration.

Organotypic Slice Culture and protocol for seeding with fibrillar α-syn polymorphs

Slice were cultured in MEM (ThermoFisher Scientific) medium supplemented with 20% heat-inactivated horse serum (Eurobio), 2mM Glutamax 100 (ThermoFisher Scientific), 1mM $CaCl_2$, 2mM $MgSO_4$, 2mM $MgCl_2$, 11mM d-Glucose, 5mM $NaHCO_3$ (ThermoFisher Scientific), and 20mM Hepes (ThermoFisher Scientific) (Cantaut-Belarif *et al*, 2017). Prior to dissection, 6-wells dishes were prepared with 900µl of culture media with a millicell insert (30mm biopore PTFE membrane, type-CM, 0.4µm, Millipore). Hippocampi were dissected from P3–P5 C57BL/6 mice and kept on ice in PBS(1X) – Glucose (1X) solution. Hippocampi were sliced (400µm) using a McIllwain tissue chopper (Mickle Laboratory) and separated in the pre-warm culture medium. 4-6 slices were plated on Millicell inserts in each 6-well dishes. Slices were maintained for 28 days with medium changed twice a week. Exposure to α-syn fibrillar polymorphs was performed on day 14. Fibrillar α-syn polymorphs were diluted in fresh culture medium and applied on top of the slices for 15min, followed by 3-washes with culture medium. The millicells were then transferred to new 6-well dishes containing fresh medium. Microglial cells were depleted using colony-stimulating factor 1 receptor (CSF1R) inhibitor, PLX3397. The inhibitor was supplemented in the culture medium (10µM) starting from day 7, until the end of the experiment, i.e. day 28. Notably, by day 14, when fibrillar α-Syn exposure was performed, microglial cells were completely depleted.

Exposure concentrations

The fibrillar polymorphs concentration is expressed throughout the work as monomer-equivalent concentration. The amount of aggregated α-Syn within all fibrillar polymorphs was determined by ultracentrifugation and measurement of the amount of monomeric α-Syn in the supernatant. The fibrillar assemblies were fragmented to the similar size (**Figure 1A-**

B). In primary neurons, short-term experiments (binding and dynamics) were performed at 50nM concentration. Seeding experiments were performed at 250nM (15min exposure, followed by wash) because no seeding was detected for Fibril-polymorph at 50nM concentration. For organotypic slices, seeding experiments were performed at 750nM and 1500nM (15min exposure, followed by wash). Control conditions refer to 1X PBS buffer exposure.

Primary Neuronal Culture and protocol for seeding with fibrillar α-syn polymorphs

Primary neuronal culture was performed as described previously (Shrivastava *et al*, 2015, 2013; Renner *et al*, 2010). Freshly dissociated (trypsin) hippocampi were plated (10^5 cells/well in a 12-well dish containing 18-mm coverslip) in neuronal attachment media consisting of 10% horse serum (Eurobio), 1mM sodium pyruvate (ThermoFisher Scientific), 2mM Glutamax-100X (ThermoFisher Scientific) and Penicillin/streptomycin (ThermoFisher Scientific) in MEM (ThermoFisher Scientific) for 3 h. The attachment medium was replaced and cells were maintained in serum-free Neurobasal medium (ThermoFisher Scientific) supplemented with B27 (GIBCO) and 2mM Glutamax-100X. Exposure to fibrillar α-syn polymorphs was performed at DIV14. Fibrillar α-syn polymorphs were diluted in fresh neurobasal medium. The "cell-conditioned neurobasal medium" was replaced with fibrillar α-syn containing neurobasal medium for 15min, the former kept aside at 37°C. After 15 min exposure, fibrillar α-syn-containing medium was removed and the well was washed thrice. Lastly the cells were replenished with "cell-conditioned neurobasal medium" and transferred back to the incubator until DIV21.

Immunolabeling, antibodies used and quantifications

Immunolabeling was performed as per standard protocol. The antibodies are listed in the table below. For organotypic slices, staining was performed on free-floating sections. For this, slices were detached from Millicells followed by blocking (0.25% gelatin and 0.2% Triton X-100 in 1X PBS) for 45 min. Slices were then incubated overnight with the appropriate primary antibodies diluted in 0.125% gelatin and 0.2% Triton-X-100 in 1X PBS. Following 3 washes (20 min each), slices were incubated with secondary antibodies (1:1000, 3 hr). After washing for 2-3h, sections were mounted onto glass slides using Vectashield (Vector Labs). Images were acquired using a Leica confocal TCS SP8 microscope and processed using ImageJ, Metamorph (Molecular Devices) and Matlab.

For primary neurons, blocking (3% BSA in 1X PBS) was performed for 30 min post permeabilization (0.2% Triton X-100 in 3% BSA in 1X PBS, 10min). No permeabilization step was required for methanol-fixation. Cells were then incubated in appropriate primary antibodies diluted in 3% BSA in 1X PBS for 1h. Following 3 washes (10 min each), slices were incubated with secondary antibodies (1:400, 45min). After 3-washes (20min), sections were mounted onto glass slides using Vectashield (Vector Labs). Images were acquired using Leica Inverted Spinning Disk microscope (DM5000B, Coolsnap HQ2 camera, Cobolt lasers).

Primary Antibody	Host	Supplier	Fixation Protocol	Dilution
Organotypic Slices				
pS129-α-Syn (81A)	Mouse Monoclonal	Millipore MABN826	4%PFA 4°C 45min	1:1200
p62/Sequestosome-1	Rabbit PolyclonalPolyclonal	Proteintech 55274-1-AP		1:1000
NeuN (Neurons)	Mouse Monoclonal	Millipore MAB377		1:800
Iba1	Rabbit Polyclonal	Wako		1:1000
Olig2	Rabbit Polyclonal	Millipore AB9610		1:500
Primary Neurons				
pS129-α-Syn (81A)	Mouse Monoclonal	Millipore MABN826	4%PFA RT 10min	1:1200
p62/Sequestosome-1	Rabbit Polyclonal	Abcam ab51253		1:1000
Tau (Axons)	Rabbit Polyclonal	Synaptic System 314 003		1:1200
α3-Na^+/K^+-ATPase	Mouse Monoclonal	ThermoFisher MA3-915		1:800
mGluR5	Rabbit Polyclonal	Millipore AB5675		1:1200
vGluT1	Guinea Pig Polyclonal	Millipore AB5905		1:1000
GluA1-AMPA	Rabbit Polyclonal	Synaptic System 182 003	Methanol -20°C 10min	1:1200
GluA2-AMPA	Rabbit Polyclonal	Synaptic System 182 103		1:1200
GluN2B-NMDA	Mouse Monoclonal	NeuroMab 75-101		1:200

Thresholding is based on wavelet based segmentation as previously described (Bannai *et al*, 2015; Shrivastava *et al*, 2015; Renner *et al*, 2010; Shrivastava *et al*, 2013). Individual structures were identified (e.g. p129-α-Syn aggregates, receptor and synaptic clusters) to generate background free masks. The fluorescence intensity of the original images on top of these masks were then computed. For p129-α-Syn, the sum of "intensity of all structures" was

calculated. Two color analysis: "*Co-localization"* is defined when there was an overlap between the thresholded clusters of two images. "*Intensity of cluster*" is defined as total fluorescence intensity per cluster. For each image the values of all clusters were averaged within the field.

Endocytosis Assay

In order to distinguish between cell surface and internalized spots, α-Syn fibrils were tagged with Biotin + ATTO488 dyes. Neuronal conditioned medium was removed (stored at 37°C) and replaced with fresh Neurobasal culture medium 15min before exposure. Live neurons were exposed with fibrillar polymorphs for 1h in incubator followed by 3-washes with pre-warmed culture medium. The cells were allowed to recover (4h or 8h) or not (0h) in neuronal conditioned medium. At the end of each time point, cells were fixed using cold 4% PFA on ice to prevent membrane rupture due to fixation. Cell surface Biotin + ATTO488 were revealed using Streptavidin555 (1:1000, 10min) followed by extensive washes. Spots positive for Biotin- Streptavidin555 and ATTO488 are localized at the cell surface, while ATTO488 only spots represent endocytosed spots. Quantification was performed as described in previous paragraph.

Sarkosyl Extraction

Neurons were plated on 10-cm dish and exposed to α-Syn polymorphs (250nM) on DIV14 and harvested on DIV21. Cells were washed 1-time in ice-cold PBS (1X) and then scrapped scraped in 1ml 1XPBS. The cells were pelleted and 500µl extraction buffer was added. Extraction buffer was composed of 20 mM Tris-HCl, pH 7.5; 0.8 M NaCl, 1 mM EGTA; 10% [w/v] sucrose and 1% sarkosyl supplemented with protease (Roche) and phosphatase (Sigma) inhibitor cocktails as described recently(Gribaudo *et al*, 2019). The cell suspension was incubated at 37°C gently shaking at 300rpm for 30min and then centrifuged at 1000rpm for 20min. The supernatant was collected and probed by western blotting. 12% gels without stacking layer were used. Following antibodies were used: p129-α-Syn (81A, Millipore / MABN826, 1:1000); Mouse specific α-Syn (D37A6, Cell Signaling / 4179S, 1:1000), Tubulin (DM1A, Abcam/ Ab7291, 1:2500).

Stochastic Optical Reconstruction Microscopy (STORM) Imaging and Quantifications

STORM imaging was performed on exogenous fibrillar α-Syn polymorphs labeled with ATTO647N or on endogenous mouse p129-α-Syn inclusions labeled with mouse-monoclonal antibody (Primary antibody:81A, Secondary antibody: Alexa 647). Imaging was performed under reducing condition with buffer composed of PBS (pH 7.4), glucose (10%), β-mercaptoethylamine (10 mM), glucose oxidase (0.5 mg/ml), and catalase (40 mg/ml), and deoxygenized with nitrogen (Shrivastava *et al*, 2015). A total of 20,000 (ATTO647N) or 40,000 (Alexa647) frames were acquired. STORM imaging was carried out on an inverted Nikon Eclipse Ti microscope equipped with a 100X oil- immersion objective (N.A. 1.49 with a microscope-inbuilt 1.5X lens) using an Andor iXon EMCCD camera (image pixel size, 106 nm). ATTO647N/Alexa647 were imaged using laser 639 nm (1 kW, used at 500 mW) for a 50 ms exposure time. Single molecules were detected and rendered with a pointing accuracy of 10nm (Gausssian radius, 10nm) using Matlab. All the quantifications were performed using open-source softwares, ImageJ and Lama (Malkusch & Heilemann, 2016), the latter was used to compute DBSCAN algorithm (Ester *et al*, 1996). DBSCAN allows the identification of clusters in large spatial data sets by looking at the local density of points. Here, after correcting for multiple detections in consecutive frames, 'density threshold' of minimum 20 detections within a radial distance of 20 nm was used.

For SPT-STORM, neurons were exposed to PA-JF-646 (Photoactivable Janelia Farm 647) labeled α-Syn polymorphs (50nM). Imaging was performed within 10-min of exposure to study the dynamic properties of fibrillar assemblies at the membrane. These photoactivable (off to on) dyes are excellent for live-cell imaging, especially in SPT experiments where they enable longer observations and better localization of individual fluorescent conjugates (Grimm *et al*, 2016). Exposure and recording were performed in Krebs recording medium (110 mM NaCl, 4 mM KCl, 1.5 mM CaCl2, 1.2 mM MgSO4, 25 mM NaHCO3, 1 mM NaH2PO4, 20 mM HEPES, 10 mM Glucose, pH 7.4). Imaging was performed as recently described(Shrivastava *et al*, 2019). PA-JF646 were acquired at 50 Hz (20 ms) using laser 647 nm (0.5 kW, used at 200-300 mW) while pulse-activating with 405 nm laser (100 mW power, used at 2–5 mW) for 6,000 frames.

Hidden Markov model

The most probable model of diffusive states was inferred by a modified version of vbSPT analysis software (Persson *et al*, 2013), which applies a Bayesian treatment of hidden Markov models. This approach was recently implemented in our work to track membrane proteins

(Shrivastava *et al*, 2019). The number of trajectories analyzed were (each experiment): Fibrils: 2982, 21202, 12041; Ribbons: 17322, 26941, 33225; Fibril-91: 11237, 12694, 45426. We assume that α-Syn single molecules remain in a steady-state within the short experimental observation time. This takes into account i) binding of new molecules to the membrane ii) cluster formation iii) dissociation of single molecules from clusters and targeting to endocytosis compartments. The analysis vbSPT method uses a maximum-evidence criterion to determine the most probable number of diffusive states from each set of observed data (n=3 experiments). The script was let to freely choose between models with one, two or three possible states. Only the position coordinates of the molecules in two successive time points were taken into account to construct the model. Based on our previous data (Shrivastava *et al*, 2019), prior values of D and dwell time were 0.1 $\mu m^2/s$ and 50 frames (1,000 ms), respectively. The minimum length of trajectory was 2.

Multi Electrode Array Recordings

Primary neuronal cultures were grown on 120 electrodes MEA plates (120MEA30/10iR-ITO, MultiChannel Systems, Reutlingen, Germany) at a density of 240,000 cells/plate. Neuronal activity was sampled at 10 kHz using MultiChannel Experimenter software and MEA2100-System (MultiChannel Systems, Reutlingen, Germany). Cells were kept in their culture medium during recordings. In these conditions, cultured neurons maintain the same network activity for at least 60 min. To avoid movement-induced artefacts, recordings were started 15 min after translocation of MEAs from incubator to the recording stage. Analysis was carried out on 10 min long sessions for each plate. Spikes, considered as point processes, were detected (± 6 SDs) in high-pass (300 Hz) filtered records. MEA plates were immediately put back in the incubator after recording. Channels with the mean firing rate < 0.1 Hz were considered as non-spiking and discarded from further analyses. Signal processing and all analyses of neuronal activity were carried out using homemade software in Matlab (The Mathworks).

In order to compare the effect of treatments on network activity, the activity of 14 DIV cultures grown on MEA was recorded as above. After recording, cultures were let to recover at least 2h in the incubator before application of fibrillar polymorphs. One week later, MEA plates were recorded again. Results are expressed as the normalized ratio of change between

14 DIV and 21 DIV to account for the inherent differences in network development between MEAs.

Graphs and Statistics

Image analysis were performed on ImageJ, Matlab. Graphs were plotted and statistics performed on GraphPad Prism software. All plots show the distribution of values as Box-plot and detailed within the legend. Dot plots shows the averaged value per experiment. When both box-plot and dot-plot are shown, the statistical test is performed on the box-plot data. Non-parametric Mann-Whitney has been performed to compare the distribution and tests whether the median of two groups are independent of each other.

Author Contribution

Conceived the project, Designed experiment: ANS, RM

Performed Experiments and Analyzed Data, ANS, LB, MR, JS, VR

Provided Resources, Funding and Equipment: RM, AT

Wrote the manuscript, ANS, AT, RM

Competing Interests

The authors declare no conflict of interest. A.N.S. is currently an employee at U.C.B. Biopharma SRL.

Fundings

The authors thank Tracy Bellande and Margaux Petay for expert technical assistance. This work was supported by Grants from the EC Joint Programme on Neurodegenerative Diseases (TransPathND, ANR-17-JPCD-0002-02), the Centre National de la Recherche Scientifique, The Fondation pour la Recherche Médicale (Contract DEQ 20160334896), a "Coup d'Elan a la Recherche Francaise" award from Fondation Bettencourt-Schueller, the Fondation Simone et Cino Del Duca of the Institut de France, the European Union's Horizon 2020 research and innovation programme and EFPIA Innovative Medicines Initiative 2 under grant agreements No. 116060 (IMPRiND) and No. 821522 (PD-MitoQUANT), an ERC advanced research grant (PLASLTINHIB), and the ''Investissements d'Avenir'' program (ANR-10-LABX-54 MEMO LIFE and ANR-11-IDEX-0001-02 PSL Research University). This work benefited from the JiePie research award attributed to RM, the electron microscopy facility Imagerie-Gif and the proteomic facility SICaPS. The opinions expressed and arguments employed herein do not necessarily reflect the official views of any funding body. We thank Luke D Lavis for providing Janelia Farm dyes and Maria J Pinto for assistance in slice culture work.

References

Abounit S, Bousset L, Loria F, Zhu S, de Chaumont F, Pieri L, Olivo-Marin J-C, Melki R & Zurzolo C (2016) Tunneling nanotubes spread fibrillar α-synuclein by intercellular trafficking of lysosomes. *EMBO J.* **35:** 2120–2138

Aguzzi A, Heikenwalder M & Polymenidou M (2007) Insights into prion strains and neurotoxicity. *Nat. Rev. Mol. Cell Biol.* **8:** 552–61

Bannai H, Niwa F, Sherwood MW, Shrivastava AN, Arizono M, Miyamoto A, Sugiura K, Lévi S, Triller A & Mikoshiba K (2015) Bidirectional Control of Synaptic GABAAR Clustering by Glutamate and Calcium. *Cell Rep.* **13:** 2768–80 Available at: http://www.ncbi.nlm.nih.gov/pubmed/26711343

Bäuerlein FJB, Saha I, Mishra A, Kalemanov M, Martínez-Sánchez A, Klein R, Dudanova I, Hipp MS, Hartl FU, Baumeister W & Fernández-Busnadiego R (2017) In Situ Architecture and Cellular Interactions of PolyQ Inclusions. *Cell* **171:** 179-187.e10

Blumenstock S, Rodrigues EF, Peters F, Blazquez-Llorca L, Schmidt F, Giese A & Herms J (2017) Seeding and transgenic overexpression of alpha-synuclein triggers dendritic spine pathology in the neocortex. *EMBO Mol. Med.* **9:** 716–731

Bousset L, Pieri L, Ruiz-Arlandis G, Gath J, Jensen PH, Habenstein B, Madiona K, Olieric V, Böckmann A, Meier BH & Melki R (2013) Structural and functional characterization of two alpha-synuclein strains. *Nat. Commun.* **4:** 2575

Braak H, Del Tredici K, Rüb U, de Vos RAI, Jansen Steur ENH & Braak E (2003) Staging of brain pathology related to sporadic Parkinson's disease. *Neurobiol. Aging* **24:** 197–211

Brahic M, Bousset L, Bieri G, Melki R & Gitler AD (2016) Axonal transport and secretion of fibrillar forms of α-synuclein, Aβ42 peptide and HTTExon 1. *Acta Neuropathol.* **131:** 539–48 Available at: http://www.ncbi.nlm.nih.gov/pubmed/26820848

Brundin P, Melki R & Kopito R (2010) Prion-like transmission of protein aggregates in neurodegenerative diseases. *Nat. Rev. Mol. Cell Biol.* **11:** 301–7

Cantaut-Belarif Y, Antri M, Pizzarelli R, Colasse S, Vaccari I, Soares S, Renner M, Dallel R, Triller A & Bessis A (2017) Microglia control the glycinergic but not the GABAergic synapses via prostaglandin E2 in the spinal cord. *J. Cell Biol.* **216:** 2979–2989

Choquet D & Triller A (2013) The Dynamic Synapse. *Neuron* **80:** 691–703 Available at: http://www.ncbi.nlm.nih.gov/pubmed/24183020 [Accessed December 8, 2019]

Elmore MRP, Najafi AR, Koike MA, Dagher NN, Spangenberg EE, Rice RA, Kitazawa M, Matusow B, Nguyen H, West BL & Green KN (2014) Colony-stimulating factor 1 receptor signaling is necessary for microglia viability, unmasking a microglia progenitor cell in the adult brain. *Neuron* **82:** 380–397

Ester M, Kriegel H-P, Sander J & Xu X (1996) A density-based algorithm for discovering clusters in large spatial databases with noise. In *KDD'96 Proceedings of the Second International Conference on Knowledge Discovery and Data Mining* pp 226–231. Portland, Oregon

Falsig J, Sonati T, Herrmann US, Saban D, Li B, Arroyo K, Ballmer B, Liberski PP & Aguzzi A (2012) Prion pathogenesis is faithfully reproduced in cerebellar organotypic slice cultures. *PLoS Pathog.* **8:** e1002985

Ferreira DG, Temido-Ferreira M, Vicente Miranda H, Batalha VL, Coelho JE, Szegö ÉM, Marques-Morgado I,

Vaz SH, Rhee JS, Schmitz M, Zerr I, Lopes LV. & Outeiro TF. (2017) α-synuclein interacts with PrPC to induce cognitive impairment through mGluR5 and NMDAR2B. *Nat. Neurosci.* **20:** 1569–1579

Flavin WP, Bousset L, Green ZC, Chu Y, Skarpathiotis S, Chaney MJ, Kordower JH, Melki R & Campbell EM (2017) Endocytic vesicle rupture is a conserved mechanism of cellular invasion by amyloid proteins. *Acta Neuropathol.* **134:** 629–653

Freundt EC, Maynard N, Clancy EK, Roy S, Bousset L, Sourigues Y, Covert M, Melki R, Kirkegaard K & Brahic M (2012) Neuron-to-neuron transmission of α-synuclein fibrils through axonal transport. *Ann. Neurol.* **72:** 517–24

Ghee M, Melki R, Michot N & Mallet J (2005) PA700, the regulatory complex of the 26S proteasome, interferes with alpha-synuclein assembly. *FEBS J.* **272:** 4023–33

Goniotaki D, Lakkaraju AKK, Shrivastava AN, Bakirci P, Sorce S, Senatore A, Marpakwar R, Hornemann S, Gasparini F, Triller A & Aguzzi A (2017) Inhibition of group-I metabotropic glutamate receptors protects against prion toxicity. *PLoS Pathog.* **13:** 1–29

Gribaudo S, Tixador P, Bousset L, Fenyi A, Lino P, Melki R, Peyrin J-M & Perrier AL (2019) Propagation of α-Synuclein Strains within Human Reconstructed Neuronal Network. *Stem cell reports* **12:** 230–244

Grimm JB, English BP, Choi H, Muthusamy AK, Mehl BP, Dong P, Brown TA, Lippincott-Schwartz J, Liu Z, Lionnet T & Lavis LD (2016) Bright photoactivatable fluorophores for single-molecule imaging. *Nat. Methods* **13:** 985–988

Guerrero-Ferreira R, Taylor NM, Arteni A-A, Kumari P, Mona D, Ringler P, Britschgi M, Lauer ME, Makky A, Verasdonck J, Riek R, Melki R, Meier BH, Böckmann A, Bousset L & Stahlberg H (2019) Two new polymorphic structures of human full-length alpha-synuclein fibrils solved by cryo-electron microscopy. *Elife* **8:** Available at: http://www.ncbi.nlm.nih.gov/pubmed/31815671 [Accessed December 18, 2019]

Guo JL, Covell DJ, Daniels JP, Iba M, Stieber A, Zhang B, Riddle DM, Kwong LK, Xu Y, Trojanowski JQ & Lee VMY (2013) Distinct α-synuclein strains differentially promote tau inclusions in neurons. *Cell* **154:** 103–17

Hansen C, Angot E, Bergström A, Steiner J a, Pieri L, Paul G, Outeiro TF, Melki R, Kallunki P, Fog K, Li J-Y & Brundin P (2011) α-Synuclein propagates from mouse brain to grafted dopaminergic neurons and seeds aggregation in cultured human cells. *J. Clin. Invest.* **121:** 715–25

Holmes BB, DeVos SL, Kfoury N, Li M, Jacks R, Yanamandra K, Ouidja MO, Brodsky FM, Marasa J, Bagchi DP, Kotzbauer PT, Miller TM, Papy-Garcia D & Diamond MI (2013) Heparan sulfate proteoglycans mediate internalization and propagation of specific proteopathic seeds. *Proc. Natl. Acad. Sci.* **110:** E3138-3147

Ichikawa M, Muramoto K, Kobayashi K, Kawahara M & Kuroda Y (1993) Formation and maturation of synapses in primary cultures of rat cerebral cortical cells: an electron microscopic study. *Neurosci. Res.* **16:** 95–103

Ivenshitz M & Segal M (2010) Neuronal density determines network connectivity and spontaneous activity in cultured hippocampus. *J. Neurophysiol.* **104:** 1052–60

Kaufman SK, Sanders DW, Thomas TL, Ruchinskas AJ, Vaquer-Alicea J, Sharma AM, Miller TM & Diamond MI (2016) Tau Prion Strains Dictate Patterns of Cell Pathology, Progression Rate, and Regional Vulnerability In Vivo. *Neuron* **92:** 796–812

Lau A, So RWL, Lau HHC, Sang JC, Ruiz-Riquelme A, Fleck SC, Stuart E, Menon S, Visanji NP, Meisl G, Faidi R, Marano MM, Schmitt-Ulms C, Wang Z, Fraser PE, Tandon A, Hyman BT, Wille H, Ingelsson M, Klenerman D, et al (2019) α-Synuclein strains target distinct brain regions and cell types. *Nat. Neurosci.* Available at: http://www.ncbi.nlm.nih.gov/pubmed/31792467 [Accessed December 18, 2019]

Li B, Ge P, Murray KA, Sheth P, Zhang M, Nair G, Sawaya MR, Shin WS, Boyer DR, Ye S, Eisenberg DS, Zhou ZH & Jiang L (2018a) Cryo-EM of full-length α-synuclein reveals fibril polymorphs with a common structural kernel. *Nat. Commun.* **9:** 3609 Available at: http://www.nature.com/articles/s41467-018-05971-2 [Accessed December 18, 2019]

Li Y, Zhao C, Luo F, Liu Z, Gui X, Luo Z, Zhang X, Li D, Liu C & Li X (2018b) Amyloid fibril structure of α-synuclein determined by cryo-electron microscopy. *Cell Res.* **28:** 897–903 Available at: http://www.ncbi.nlm.nih.gov/pubmed/30065316 [Accessed December 18, 2019]

Luk KC, Kehm V, Carroll J, Zhang B, O'Brien P, Trojanowski JQ & Lee VM-Y (2012) Pathological -Synuclein Transmission Initiates Parkinson-like Neurodegeneration in Nontransgenic Mice. *Science (80-.).* **338:** 949–953

Makky A, Bousset L, Polesel-Maris J & Melki R (2016) Nanomechanical properties of distinct fibrillar polymorphs of the protein α-synuclein. *Sci. Rep.* **6:** 37970

Malkusch S & Heilemann M (2016) Extracting quantitative information from single-molecule super-resolution imaging data with LAMA – LocAlization Microscopy Analyzer. *Sci. Rep.* **6:** 34486

Melki R (2015) Role of different alpha-synuclein strains in synucleinopathies, similarities with other neurodegenerative diseases. *J. Parkinsons. Dis.* **5:** 217–227

Melki R (2017) The multitude of therapeutic targets in neurodegenerative proteinopathies. In *Disease-Modifying Targets in Neurodegenerative Disorders* pp 1–20. Elsevier

Melki R (2018) How the shapes of seeds can influence pathology. *Neurobiol. Dis.* **109:** 201–208

Mougenot A-L, Nicot S, Bencsik A, Morignat E, Verchère J, Lakhdar L, Legastelois S & Baron T (2012) Prion-like acceleration of a synucleinopathy in a transgenic mouse model. *Neurobiol. Aging* **33:** 2225–8

Peelaerts W, Bousset L, Van der Perren A, Moskalyuk A, Pulizzi R, Giugliano M, Van den Haute C, Melki R & Baekelandt V (2015) α-Synuclein strains cause distinct synucleinopathies after local and systemic administration. *Nature* **522:** 340–4

Persson F, Lindén M, Unoson C & Elf J (2013) Extracting intracellular diffusive states and transition rates from single-molecule tracking data. *Nat. Methods* **10:** 265–269

Prusiner SB, Woerman AL, Mordes DA, Watts JC, Rampersaud R, Berry DB, Patel S, Oehler A, Lowe JK, Kravitz SN, Geschwind DH, Glidden D V., Halliday GM, Middleton LT, Gentleman SM, Grinberg LT & Giles K (2015) Evidence for α-synuclein prions causing multiple system atrophy in humans with parkinsonism. *Proc. Natl. Acad. Sci.* **112:** E5308–E5317

Renner M, Lacor PN, Velasco PT, Xu J, Contractor A, Klein WL & Triller A (2010) Deleterious Effects of Amyloid β Oligomers Acting as an Extracellular Scaffold for mGluR5. *Neuron* **66:** 739–754

Rey NL, Steiner JA, Maroof N, Luk KC, Madaj Z, Trojanowski JQ, Lee VM-Y & Brundin P (2016) Widespread transneuronal propagation of α-synucleinopathy triggered in olfactory bulb mimics prodromal Parkinson's disease. *J. Exp. Med.* **213:** 1759–1778

Rodriguez JA, Ivanova MI, Sawaya MR, Cascio D, Reyes FE, Shi D, Sangwan S, Guenther EL, Johnson LM,

Zhang M, Jiang L, Arbing MA, Nannenga BL, Hattne J, Whitelegge J, Brewster AS, Messerschmidt M, Boutet S, Sauter NK, Gonen T, et al (2015) Structure of the toxic core of α-synuclein from invisible crystals. *Nature* **525:** 486–90 Available at: http://www.nature.com/articles/nature15368 [Accessed December 18, 2019]

Shrivastava AN, Aperia A, Melki R & Triller A (2017) Physico-Pathologic Mechanisms Involved in Neurodegeneration: Misfolded Protein-Plasma Membrane Interactions. *Neuron* **95:** 33–50 Available at: http://dx.doi.org/10.1016/j.neuron.2017.05.026

Shrivastava AN, Kowalewski JM, Renner M, Bousset L, Koulakoff A, Melki R, Giaume C & Triller A (2013) β-amyloid and ATP-induced diffusional trapping of astrocyte and neuronal metabotropic glutamate type-5 receptors. *Glia* **61:** 1673–86 Available at: http://www.ncbi.nlm.nih.gov/pubmed/23922225

Shrivastava AN, Redeker V, Fritz N, Pieri L, Almeida LG, Spolidoro M, Liebmann T, Bousset L, Renner M, Léna C, Aperia A, Melki R & Triller A (2015) α-synuclein assemblies sequester neuronal α3-Na+/K+-ATPase and impair Na+ gradient. *EMBO J.* **34:** 2408–23 Available at: http://www.ncbi.nlm.nih.gov/pubmed/26323479

Shrivastava AN, Redeker V, Pieri L, Bousset L, Renner M, Madiona K, Mailhes-Hamon C, Coens A, Buée L, Hantraye P, Triller A & Melki R (2019) Clustering of Tau fibrils impairs the synaptic composition of α3-Na+/K+-ATPase and AMPA receptors. *EMBO J.***:** e99871

Shrivastava AN, Triller A & Melki R (2018) Cell biology and dynamics of Neuronal Na+/K+-ATPase in health and diseases. *Neuropharmacology* **13:** e1006733 Available at: https://doi.org/10.1016/j.neuropharm.2018.12.008

Sonati T, Reimann RR, Falsig J, Baral PK, O'Connor T, Hornemann S, Yaganoglu S, Li B, Herrmann US, Wieland B, Swayampakula M, Rahman MH, Das D, Kav N, Riek R, Liberski PP, James MNG & Aguzzi A (2013) The toxicity of antiprion antibodies is mediated by the flexible tail of the prion protein. *Nature* **501:** 102–106

Strohäker T, Jung BC, Liou S, Fernandez CO, Riedel D, Becker S, Halliday GM, Bennati M, Kim WS, Lee S & Zweckstetter M (2019) Structural heterogeneity of α -synuclein fi brils ampli fi ed from patient brain extracts. **:** 1–12

Tuttle MD, Comellas G, Nieuwkoop AJ, Covell DJ, Berthold DA, Kloepper KD, Courtney JM, Kim JK, Barclay AM, Kendall A, Wan W, Stubbs G, Schwieters CD, Lee VMY, George JM & Rienstra CM (2016) Solid-state NMR structure of a pathogenic fibril of full-length human α-synuclein. *Nat. Struct. Mol. Biol.* **23:** 409–15 Available at: http://www.nature.com/articles/nsmb.3194 [Accessed December 18, 2019]

Um JW, Kaufman AC, Kostylev M, Heiss JK, Stagi M, Takahashi H, Kerrisk ME, Vortmeyer A, Wisniewski T, Koleske AJ, Gunther EC, Nygaard HB & Strittmatter SM (2013) Metabotropic Glutamate Receptor 5 Is a Coreceptor for Alzheimer A b Oligomer Bound to Cellular Prion Protein. *Neuron* **79:** 887–902

Unni VK, Weissman T a, Rockenstein E, Masliah E, McLean PJ & Hyman BT (2010) In vivo imaging of alpha-synuclein in mouse cortex demonstrates stable expression and differential subcellular compartment mobility. *PLoS One* **5:** e10589

Verasdonck J, Bousset L, Gath J, Melki R, Böckmann A & Meier BH (2016) Further exploration of the conformational space of α-synuclein fibrils: solid-state NMR assignment of a high-pH polymorph. *Biomol. NMR Assign.* **10:** 5–12

Volpicelli-Daley LA, Luk KC, Patel TP, Tanik SA, Riddle DM, Stieber A, Meaney DF, Trojanowski JQ & Lee VM-Y (2011) Exogenous α-synuclein fibrils induce Lewy body pathology leading to synaptic dysfunction and neuron death. *Neuron* **72:** 57–71

Wong YC & Krainc D (2017) α-synuclein toxicity in neurodegeneration: mechanism and therapeutic strategies. *Nat. Med.* **23:** 1–13

Rey NL, Bousset L, George S, Madaj Z, Meyerdirk L, Schulz E, Steiner JA, Melki R, & Brundin P (in press) α-Synuclein conformational strains spread, seed and target neuronal cells differentially after injection into the olfactory bulb. *Acta Neuropathol Commun*.

Gribaudo S, Tixador P, Bousset L, Fenyi A, Lino P, Melki R, Peyrin JM, & Perrier AL (2019) Propagation of α-Synuclein Strains within Human Reconstructed Neuronal Network. *Stem Cell Reports*. 12: 230-44.

Valdinocci D, Simões RF, Kovarova J, Cunha-Oliveira T, Neuzil J, & Pountney DL (2019) Intracellular and Intercellular Mitochondrial Dynamics in Parkinson's Disease. *Front Neurosci*. 13: 930.

Ordonez DG, Lee MK, & Feany MB (2018) α-synuclein Induces Mitochondrial Dysfunction through Spectrin and the Actin Cytoskeleton. i 7: 108-24.

Figure 1. Characterization of five fibrillar α-Syn polymorphs.

(**A**) Transmission electron micrographs of negatively-stained α-Syn fibrillar polymorphs Fibrils, Ribbons, Fibrils-91, Fibrils-65 and Fibrils-110 before (upper lane) and after fragmentation (lower lane).

(**B**) Length distribution of the fragmented fibrillar polymorphs. The number (n) of fibrillar assemblies the histograms were derived from is indicated.

(C) Proteinase K degradation patterns of α-Syn (100μM monomer concentration) polymorphs Fibrils, Ribbons, Fibrils-91, Fibrils-65 and the fibrillar form of the truncated form of α-Syn spanning residues 1-110 monitored over time on Coomassie stained SDS–PAGE (12%). Time (min) and molecular weight markers (kDa) are shown on the top and left of each gel, respectively.

Figure 2. Differential fibrillar α-Syn polymorphs binding and clustering on primary neuronal cultures

(A) Cultured hippocampal neurons (DIV 21-24) exposed for 5 or 60 minutes to the fibrillar α-Syn polymorphs Fibrils, Ribbons, Fibrils-91, Fibrils-65 and Fibrils-110 (50nM) labeled with ATTO550 followed by fixation and immunolabeling of Homer (excitatory post-synapse marker) (Top two row: full field view; bottom two rows: boxed region). Full field view of ATTO-550 fluorescence is shown in grey-scale (top row) for better visualization of neuronal morphology. The images reveal striking differences in binding. Fibrils-91 bound much more efficiently than Ribbons and Fibrils polymorphs. Fibrils-65 and Fibrils-110 exhibited weak binding. All three polymorphs exhibited significant co-localization with homer (bottom row).

(B-D) Quantification of size (**B**, fluorescence intensity of fibrillar ATTO550-α-Syn polymorphs clusters, density (**C**, number of fibrillar ATTO550-α-Syn polymorphs clusters per μm^2, and synaptic co-localization (**D**) of fibrillar ATTO550-α-Syn polymorphs clusters obtained after thresholding (see Material and Methods section). (**D**) The proportion of synaptic fibrillar α-Syn polymorphs clusters were similar for all polymorphs except Fibrils-65 and Fibrils-110.

Box-plot shows median, inter-quartile range and 10-90% distribution. Mann-Whitney test performed to compare the distribution between 5 min and 60 min; 60-75 images from 4-5 independent experiments. ***$p<0.001$, ns=not significant. Dot plot shows the averaged value per experiment.

Figure 3. Nanoscopic properties of the clusters fibrillar α-Syn polymorphs form on primary neuron plasma membrane

(A) Super-resolution images rendered with a pixel size of 10nm (red, top row) shows the binding/clustering of fibrillar α-Syn-ATTO647N polymorphs on neurons following 60min exposure to the fibrillar polymorphs Fibrils, Ribbons and Fibrils-91 (50nM). Bottom row (white) shows fibrillar α-Syn-ATTO647N clusters identified through the DBSCAN analysis (see Material and Methods section).

(B) Density (detections/μm^2) of single molecule events on neurons (clustered and non-clustered) in panel **A** showing differential binding of the distinct fibrillar α-Syn polymorphs.

(C) Proportion of single molecule detections within clusters showing predominantly clustered (90%) binding of the distinct fibrillar α-Syn-ATTO647N polymorphs.

(D) Measurement of area of clusters (μm^2) shown as a cumulative distribution plot and box plot (inset, n=Fibrils:7681, Ribbons: 4600, Fibrils-91:8672). The distribution shows that the fibrillar polymorph Fibrils-91 populates clusters >200000 nm^2. The cumulative plot shows that the polymorph Ribbons populates the smallest clusters (<500nm^2).

(**E-F**) Representative example showing single molecule trajectories (colored) obtained using SPT-STORM of α-Syn-PA-646 Fibrils-91 polymorph. Trajectories were analyzed by Bayesian treatment of Hidden Markov Models (see Methods) that revealed three diffusive states of α-Syn polymorphs. State 1 represents free, fast diffusing molecules; State 2 exhibit intermediate diffusion velocity, representing small complexes; State 3 represents clustered fraction with very slow-diffusion velocity.

(**G-I**) Plots showing averaged diffusion coefficient values (**G**) and Dwell-time within each diffusive state (**H**) and occupancy (**I**) for each polymorph. Note Ribbons polymorphs exhibit characteristic different diffusive behavior. Each dot represents averaged value of thousands of trajectories for a given imaging field.

Dot plot in panel **B** and **C** represents averaged value per image, n=9 cells from 3 independent experiments. Box-plot in **D** shows median, inter-quartile range and 10-90% distribution. Dot plot in panel **G** and **H** averaged value per recording (thousands of trajectories) from 3 independent. Mann-Whitney-test is performed. *p<0.05, ***p<0.001, ns= not significant. Scale bars: 1μm.

Figure 4. Assessment of time-dependent endocytosis of α-Syn fibrillar polymorphs

(A) Schematic representation of the experimental setup to measure the initial endocytosis of fibrillar α-Syn polymorphs. Neurons were exposed (50nM, 60min) to ATTO488 + Biotin-labeled α-Syn. Unbound assemblies were next washed away. Cells were fixed 0h, 4h or 8h after exposure to fibrillar α-Syn polymorphs (green) and α-Syn clusters remaining on cell-surface were labeled with streptavidin-550 (red).

(**B**) Representative raw (top panel) and thresholded (bottom panel) images for α-Syn fibrillar polymorph Fibrils labeled with ATTO488 (green) and Biotin are shown. α-Syn Fibrils remaining on cell surface were labeled with streptavidin-550 (red). The majority of α-Syn clusters were on cell-surface (overlay, yellow). Internalized fibrillar α-Syn spots (green only) was quantified and plotted in panel C.

(**C**) A time-dependent increase in fibrillar α-Syn polymorphs endocytosis is observed.

Box-plot shows median, inter-quartile range and 10-90% distribution. Mann-Whitney test performed to compare the distributions; 30 images from 3 independent experiments. ***p<0.001, **p<0.01, *p<0.05, ns=not significant. Dot plot shows the averaged value per experiment.

Figure 5. Differential seeding by fibrillar α-Syn polymorphs in primary neuronal cultures

(A) Schematic representation of the protocol used to assess the seeding of endogenous α-Syn by exogenous fibrillar α-Syn polymorphs Fibrils, Ribbons and Fibrils-91. Primary mature hippocampal cultured neurons (prepared from wild-type C57BL6J mice) were exposed to fibrillar α-Syn polymorphs (250nM, 15 min in fresh culture medium) at DIV 14. After extensive washing, the cells were transferred back to the original culture medium. Neurons were fixed at DIV 21 and immunolabeled for pS129-α-Syn.

(**B**) Seeded endogenous α-Syn aggregation following exposure of primary neuronal cultures to the fibrillar α-Syn polymorphs Fibrils, Ribbons and Fibrils-91 imaged using the monoclonal anti-pS129-α-Syn antibody 81A.

(**C**) Quantification of the area occupied by aggregated pS129-α-Syn following exposure to the different fibrillar α-Syn polymorphs. Box-plot shows median, inter-quartile range and 10-90% distribution. Number of images (n): Fibrils, 30; Ribbons, 34; Fibrils-91, 34, from 3 independent experiments; Mann-Whitney-test is performed, ***p<0.001. Dot plot shows the averaged value per experiment.

(D) Seeded endogenous pS129-α-Syn (green) within axons (red, labelled with anti tau antibody).

(E) pS129-α-Syn bundles (green) are stained by the autophagy marker p62 (red) in the cell body but not in the processes (arrows).

(**F**) pS129-Syn bundles (green) are stained by the ubiquitin (red).

(**G**) 1% Sarkosyl extract from unseeded or polymorph-seeded neurons. Western blots following migration of extracts on SDS-PAGE gels without stacking layer and probing for

pS129-α-Syn (left), endogenous mouse α-Syn (middle) and tubulin (right). * represents the correct detected bands. Aggregated pS129-α-Syn can be detected in Ribbon/Fibril-91 seeded neurons (left and middle). Soluble endogenous mouse α-Syn is detected in all conditions (middle).

Figure 6. Seeded pS129-α-Syn are composed of multiple intertwined elongated structures

(**A-C**) Super-resolution STORM imaging of endogenous pS129-α-Syn was performed at DIV 21 following exposure of primary neuronal cultures to the fibrillar α-Syn polymorphs Fibrils, Ribbons and Fibrils-91 (250nM) for 15 minutes on DIV 14. Single molecule detections for 40,000 frames, rendered with a pixel size of 10nm are shown for Fibrils (**A**), Ribbons (**B**) and Fibrils-91 (**C**). In all three cases, elongated structures that seem to intertwine into larger bundles are seen.

(D) Time course of elongated and intertwined pS129-α-Syn structures formation imaged by STORM after exposure of primary neurons to α-Syn fibrillar polymorph Fibrils-91 after2 days, 3 days and 6 days.

(E-F) Quantitative analysis of the amount of elongated and intertwined pS129-α-Syn structures forming in primary neurons exposed to fibrillar α-Syn polymorphs (250nM for 15min on DIV 14) as a function of time. Detection events within (**E**) and area occupied by (**F**) pS129-α-Syn aggregates. Box-plot shows median, inter-quartile range and 10-90% distribution. Mann-Whitney test performed to compare the distributions; n is number of pS129-α-Syn aggregates analyzed: 40 for Fibrils, 52 for Ribbons, 56 for Fibrils-91. ***p<0.001, **p<0.01, *p<0.05. Scale bars: 500nm.

Figure 7. Differential α-Syn polymorphs binding and seeding in organotypic slice cultures

(A-B) Hippocampal organotypic slices maintained for 14 days in culture (day 0) were exposed to 1.5µM ATTO550-labeled fibrillar α-Syn polymorphs Fibrils, Ribbons and Fibrils-91 for 15min, washed extensively and transferred to a fresh slice culture medium for 1h prior to fixation. (**A**) Representative confocal images are shown for the fibrillar α-Syn polymorphs Fibrils, Ribbons and Fibrils-91. (**B**) Quantification of fibrillar ATTO550-α-Syn polymorphs fluorescence intensity.

Box-plot shows median, inter-quartile range and 10-90% distribution. Mann-Whitney test is performed. Number of images analyzed (n): 16 for Fibrils, 16 for Ribbons, 12 for Fibrils-91 from 3 independent experiments. *p<0.05, **p<0.01, ***p<0.001. Scale bars: 5µm.

(C) Schematic representation of the protocol used to assess the seeding of endogenous α-Syn by exogenous fibrillar α-Syn polymorphs Fibrils, Ribbons and Fibrils-91. Hippocampal

organotypic slices maintained for 14 days in culture (day 0) were exposed to 0.75 or 1.5µM ATTO550-labeled fibrillar α-Syn polymorphs for 15min, washed extensively and transferred to a fresh slice culture medium. Slices were fixed at different days and stored at 4°C until the end of experiment when immunohistochemistry for pS129-α-Syn was performed.

(D-F) Representative images (**D**) showing seeded endogenous pS129-α-Syn labeled with the antibody 81A (green, top row), exogenous-α-Syn-ATTO550 (red, applied at 0.75µM, middle row) and overlaid channels (bottom row) following exposure of hippocampal organotypic slices to fibrillar α-Syn polymorphs Fibrils, Ribbons and Fibrils-91. The percentage of area occupied by pS129-α-Syn was plotted in **E** and total fluorescence of exogenous-α-Syn-ATTO550 was plotted in **F**. Box-plot shows median, inter-quartile range and 10-90% distribution. Mann-Whitney test performed to compare the difference from Day 4 for each polymorphs; number of images (n) acquired with inclusions from 3-5 experiments (left to right): 10, 3, 4, 29, 3, 5, 37, 9 12 22. *p<0.05, **p<0.0.01, ***p<0.001, ns= not significant.

(G) Aggregated bundles of endogenous pS129-α-Syn structures (green) within neuronal cell body (grey, labelled with anti NeuN antibody).

(H) pS129-α-Syn bundles (green) are stained by the autophagy marker p62 (red) in neurons cell bodies not in the processes (arrows).

(**I-J**) Concentration-dependent seeding of endogenous α-Syn aggregation. Hippocampal organotypic slices were exposed on day 0 to fibrillar α-Syn-ATTO550 polymorphs Fibrils, Ribbons and Fibrils-91 (0.75µM or 1.5µM) and immunolabeled with the anti-pS129-α-Syn antibody 81A on day 14 (**F**). Quantification of percentage area occupied by pS129-α-Syn (**G**). Box-plot shows median, inter-quartile range and 10-90% distribution. Mann-Whitney test performed to compare the difference between 0.75µM and 1.5µM for each polymorphs; number of images acquired from 4 experiments (left to right): 16, 27, 22, 35, 25, 31. *p<0.05, ***p<0.001. Scale bars: 10µM

Figure 8. Differential re-distribution of synaptic α3-NKA/GluA2-AMPA/GluN2B-NMDA in primary neurons exposed to distinct α-Syn fibrillar polymorphs.

(**A-J**) Imunocytochemistry on DIV 21 of **(A)** α3-NKA (red) and Homer (green), (**C**) GluA2-AMPA receptors (red) and PSD95 (green), (**E**) GluN2B-NMDA receptors (red) and Homer (green) **(G)** GluA1-AMPA receptors (red) and PSD95 (green) and (**I**) mGluR5 receptors (red) and Homer (green). Primary neurons were exposed (15min, 250nM) to the fibrillar α-Syn polymorphs Fibrils, Ribbons and Fibrils-91 on DIV 14. Quantification of intensity of synaptic α3-NKA (**B**), GluA2-AMPA receptors (**D**) GluN2B-NMDA receptors (**F**), GluA1-AMPA receptors (**H**) and mGluR5 (**J**) clusters (indicative of size; see Material and Methods) was performed and plotted.

Box-plot shows median, inter-quartile range and 10-90% distribution. Number of images (n) analyzed and plotted: (**B**) 47 from 4 independent experiments, (**D**) 37 from 3 independent experiments, (**F**) 30 from 3 independent experiments, (**H**) 37 from 3 independent experiments, (**J**) 20 from 2 independent experiments. Mann-Whitney-test is performed. *p<0.05, **p<0.01, ***p<0.001, ns= not significant. Dot plot shows the averaged value per experiment. Scale bars: 5µM.

Figure 9. Alteration in network activity in primary neurons seeded with α-Syn fibrillar polymorphs

(**A-D**) Raster plots showing the spiking activity of primary neurons recorded using 120-electrode MEA plates seeded with fibrillar α-Syn polymorphs. Each row represents 1-electrode and each dot represents a single spike obtained on DIV 21 (seeded neurons, 1-week after exposure to α-Syn polymorphs). Notably control neurons exhibit high-spike frequency whereas fibrillar α-Syn polymorphs exposed neurons have decreased spiking frequency.

(**E**) Quantification showing the normalized ratio of change in spike frequency rate between DIV 14 and DIV 21. Nearly 60% reduction in the spike-frequency rate is observed in polymorph Fibrils seeded neurons. Dot plot represents averaged value per experiment. Two-tailed t-test to compare difference from control condition was performed, *p = 0.0227, ns= not significant, 3-experiments.

Supplementary Figure 1. Binding of α-Syn in and out of synapses

(**A**) Exposure of neurons to fibrillar α-Syn polymorphs (image for Fibrils-91-ATTO550 is presented, red) followed by immunolabeling of excitatory pre-synaptic boutons using vGluT1 (green) antibody. Binding and clustering of α-Syn is observed both in and out of synaptic terminals.

(**B**) Binding of α-Syn polymorphs (image for Fibrils-91-ATTO550 is presented, red) on neuronal dendrite (labeled with GFP, green). Binding and clustering of α-Syn is observed both in dendritic spines and shaft.

Supplementary Figure 2. Endogenous α-Syn is phosphorylated upon exposure in primary neuronal cultures to exogenous fibrillar polymorphs

(**A-B**) Primary mature hippocampal neurons cultures were exposed to wild-type or S129A fibrillar polymorphs (Fibrils and Fibrils-91) (250nM, 15 min in fresh culture medium) at DIV 14. After extensive washing, cells were transferred back to the original culture medium. Neurons were fixed at DIV 21 and immunolabeled for pS129-α-Syn (**A**). Similar pS129-α-Syn signal was observed after exposure to wild-type or S129A fibrillar α-Syn polymorphs (**A**). Quantification of the area occupied by aggregated pS129-α-Syn using the 81A antibody following exposure to the fibrillar α-Syn polymorphs.

Box-plot shows median, inter-quartile range and 10-90% distribution. Mann-Whitney test is performed to compare the difference; number of images (n) from 2 experiments (left to right): 16, 22, 30, 30. ***p<0.001, ns= not significant.

Supplementary Figure 3. No alteration in synapse density in α-Syn seeded neurons

(**A-D**) Immunodetection of synapses using Homer antibody in primary neurons (**A**) or organotypic slices (**B**) in control or α-Syn polymorphs seeded neurons. No or subtle alteration in synaptic density was observed (**B, D**). Dot plot shows average value from 7-experiments in cultures and 4-experiments in slices; Mann-Whitney test, **p<0.01, ns= not significant.

Supplementary Figure 4. Endogenous α-Syn is phosphorylated upon exposure of organotypic slice cultures to exogenous fibrillar polymorphs

(**A-B**) Organotypic slice cultures were exposed to wild-type or S129A fibrillar polymorphs (Fibrils and Fibrils-91 polymorphs) (1.5μM, 15 min in fresh culture medium) at day 0. After extensive washing, slices were transferred to a new culture medium. Slices were fixed on day 14 and immunolabeled for pS129-α-Syn (**A**). Similar pS129-α-Syn signal was observed after exposure to wild-type or S129A fibrillar α-Syn polymorphs (**A**). Quantification of the area occupied by aggregated pS129-α-Syn using the 81A antibody following exposure to the fibrillar α-Syn polymorphs.

Box-plot shows median, inter-quartile range and 10-90% distribution. Mann-Whitney test is performed to compare the difference; number of images (n) from 2 experiments (left to right): 22, 21, 22, 23. *p<0.05, ns= not significant.

Supplementary Figure 5. Morphology of organotypic slices in seeded neurons

Low magnification images of brain slices immunostained for neuronal marker, NeuN (green) prior (control) or after exposure to α-Syn polymorphs on Day 28 in culture after addition of the fibrillar polymorphs on Day 14. No alteration in hippocampal morphology is detected.

Supplementary Figure 6. Detection of pS129-α-Syn aggregates in oligodendrocytes

Organotypic slice cultures were exposed to the fibrillar polymorphs Fibrils, Ribbons and Fibrils-91(1.5μM) at day 0. Slices were fixed on day 14 and immunolabeled for pS129-α-Syn (81A antibody) and oligodendrocyte marker (Olig 2 antibody). No pS129-α-Syn deposits in Olig2 positive cells for slices exposed to Fibrils/Fibrils-91 polymorphs was observed. Occasional pS129-α-Syn reactivity within Olig2-positive oligodendrocytes was observed for Ribbons (middle).

Supplementary Figure 7. Unaltered seeding in organotypic slices following microglia depletion

(**A-B**) Organotypic slice cultures were prepared (day -14) and exposed to α-Syn fibrillar polymorphs (1.5μM, 15 min in fresh culture medium) at day 0. After extensive washing, the slices were transferred to a new culture medium. Slices were fixed on day 14 and immunolabeled for pS129-α-Syn and Iba1. Complete microglia depletion (**A**) was achieved using PLX3397 treatment as described in Materials and Methods. Notably fibrillar polymorphs seeded the aggregation of endogenous α-Syn both in absence and presence of microglia (**A, B**). Dot-plot shows individual organotypic slice. Mann-Whitney test is

performed to compare the difference; number of slices (n=10) from 3 experiments. *p<0.05, ns= not significant.

Supplementary Figure 8. Quality control analysis of labeled α-Syn Fibrils . MALDI-TOF mass spectra, from top to bottom of (A) unlabelled, (B) ATTO480, (C) ATTO550, (D) ATTO647 and (E) biotin-labeled wild-type α-Syn Fibrils are shown. The spectra show that α-Syn is labelled on average by ≤ one ATTO480, 550, 647 or biotin molecule. Stars depict sinapinic acid matrix adducts.
For mass spectrometry analysis, the samples were de-salted (with 5% acetonitrile, 0.1% Trifluoroacetic acid (TFA)) and eluted from a C18 reversed-phase Zip-Tip (Millipore, Billerica, MA, USA) in 50% acetonitrile, 0.1% TFA. The polypeptides were mixed in a ratio of 1:5 to 1:20 (v⁄v) with sinapinic acid (10 mg/mL) in 50% acetonitrile and 0.1% TFA) and spotted (0.5 μL) on a stainless steel MALDI target (Opti-TOF; Applied BioSystems). MALDI-TOF-TOF MS spectra were acquired with a MALDI-TOF⁄TOF 5800 mass spectrometer (Applied Biosystems) using linear mode acquisition. Acquisition and data analysis were performed using the Data Explorer software from Applied Biosystems.

Figure 1

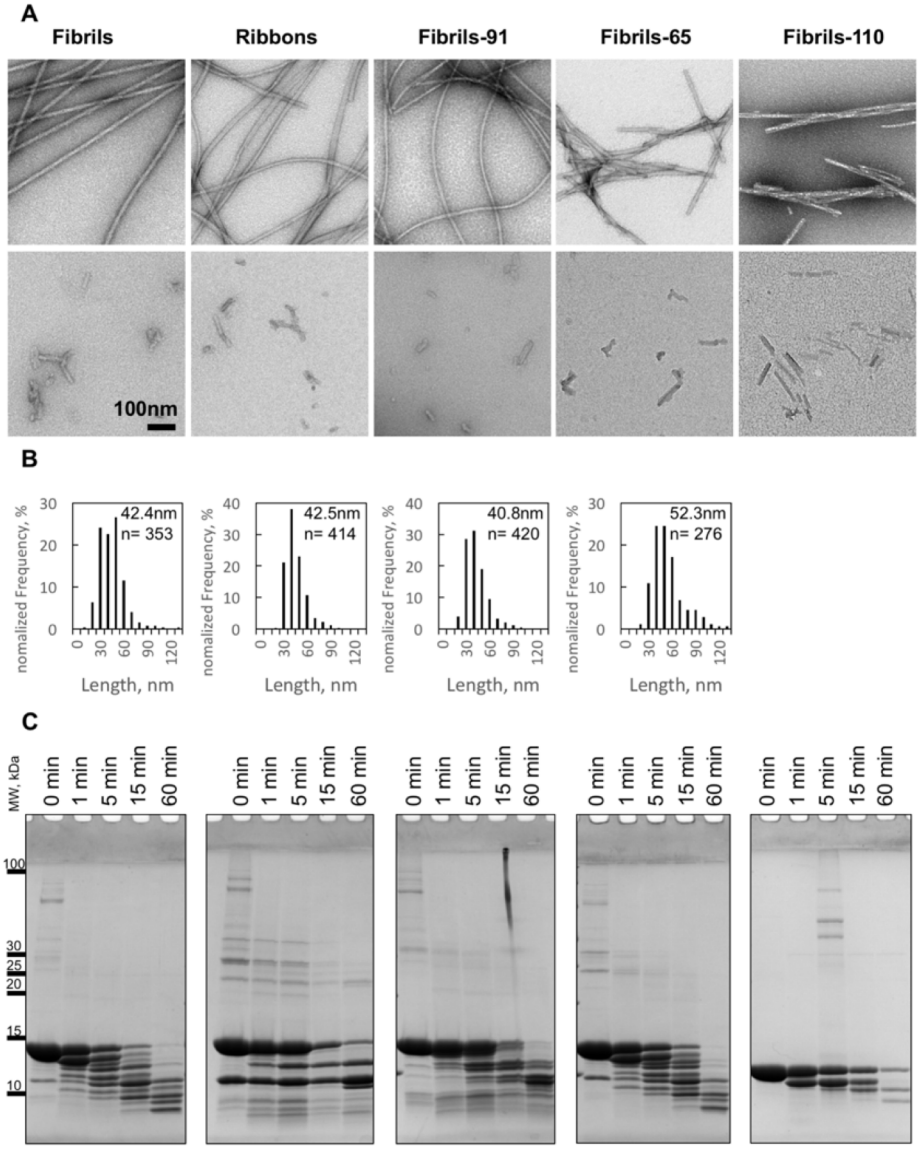
A
Fibrils
Ribbons
Fibrils-91
Fibrils-65
Fibrils-110
100nm
B
nomalized Frequency, %
42.4nm
n= 353
42.5nm
n= 414
40.8nm
n= 420
52.3nm
n= 276
Length, nm
C
MW, kDa
0 min
1 min
5 min
15 min
60 min
100
30
25
20
15
10

Figure 2

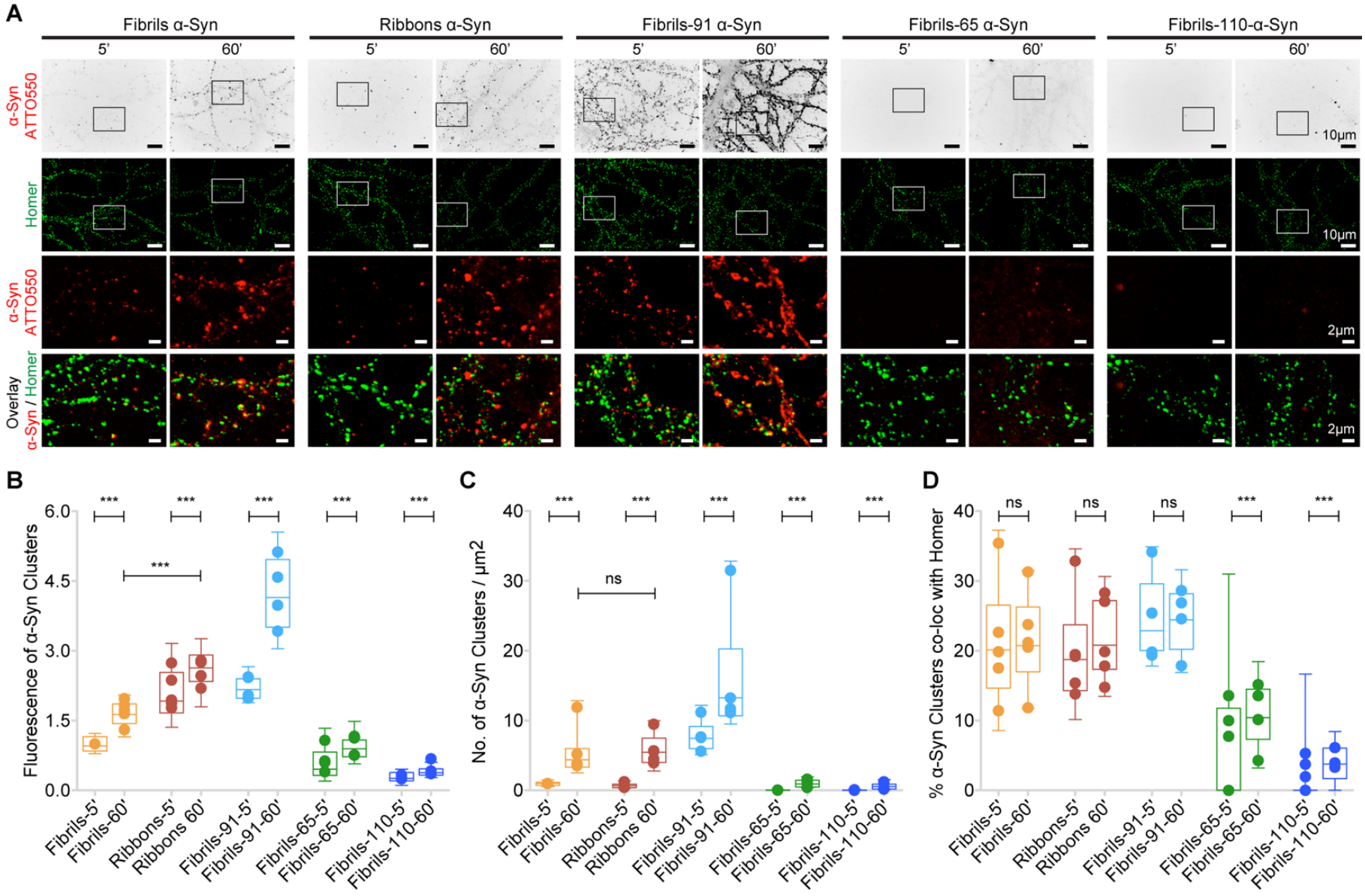
A
Fibrils α-Syn
Ribbons α-Syn
Fibrils-91 α-Syn
Fibrils-65 α-Syn
Fibrils-110-α-Syn
5'
60'
α-Syn ATTO550
Homer
Overlay α-Syn / Homer
10µm
2µm
B
Fluorescence of α-Syn Clusters
C
No. of α-Syn Clusters / µm2
D
% α-Syn Clusters co-loc with Homer
***
ns
Fibrils-5'
Fibrils-60'
Ribbons-5'
Ribbons 60'
Fibrils-91-5'
Fibrils-91-60'
Fibrils-65-5'
Fibrils-65-60'
Fibrils-110-5'
Fibrils-110-60'

Figure 3

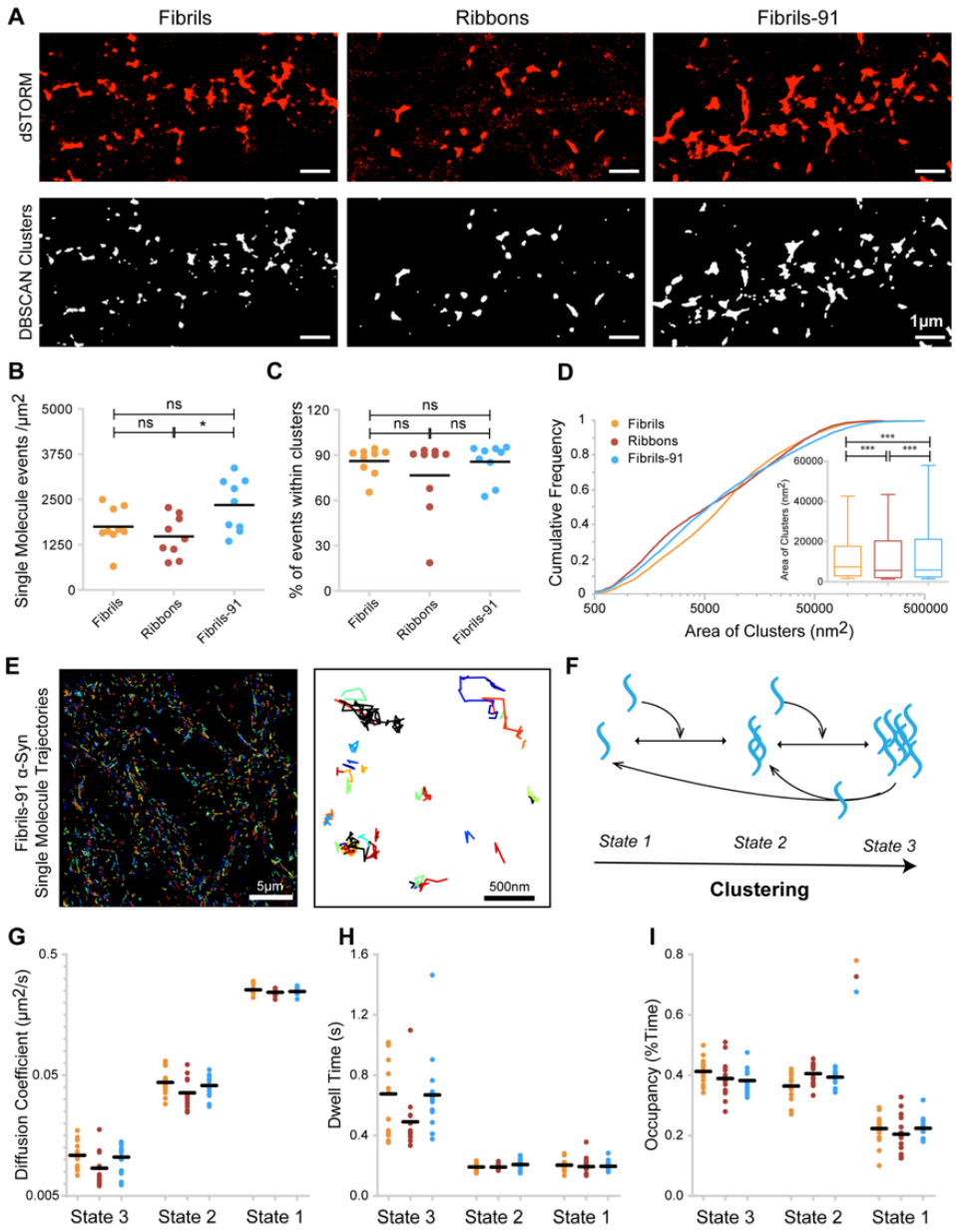
A
Fibrils
Ribbons
Fibrils-91
dSTORM
DBSCAN Clusters
1µm
B
Single Molecule events /µm2
ns
ns
*
Fibrils
Ribbons
Fibrils-91
C
% of events within clusters
ns
ns
ns
D
Cumulative Frequency
Fibrils
Ribbons
Fibrils-91
Area of Clusters (nm2)
E
Fibrils-91 α-Syn
Single Molecule Trajectories
5µm
500nm
F
State 1
State 2
State 3
Clustering
G
Diffusion Coefficient (µm2/s)
State 3
State 2
State 1
H
Dwell Time (s)
State 3
State 2
State 1
I
Occupancy (%Time)
State 3
State 2
State 1

Figure 4

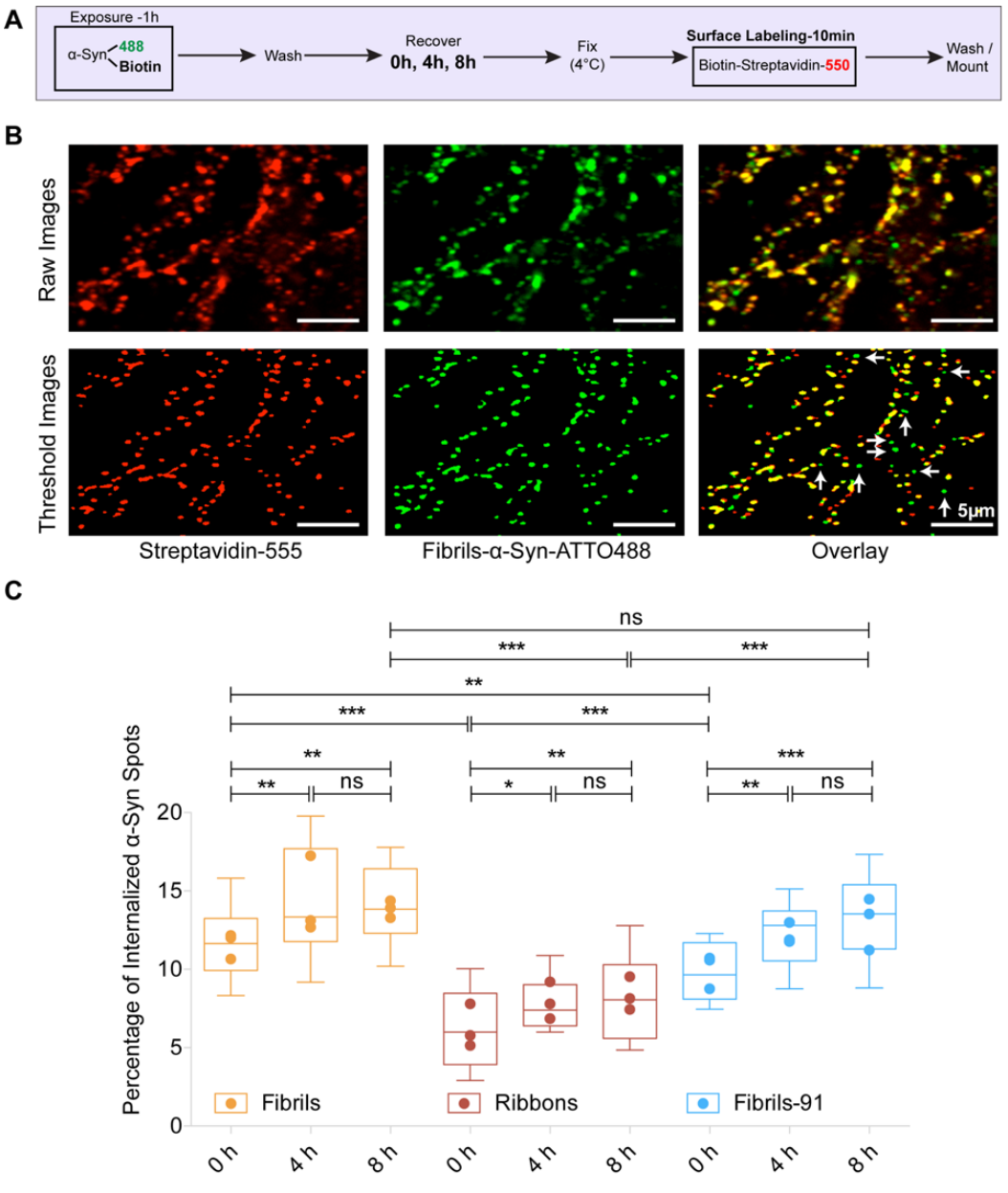
A
Exposure -1h
α-Syn 488
Biotin
Wash
Recover
0h, 4h, 8h
Fix
(4°C)
Surface Labeling-10min
Biotin-Streptavidin-550
Wash / Mount
B
Raw Images
Threshold Images
5µm
Streptavidin-555
Fibrils-α-Syn-ATTO488
Overlay
C
Percentage of Internalized α-Syn Spots
Fibrils
Ribbons
Fibrils-91
0 h
4 h
8 h
ns
***
**
*

Figure 5

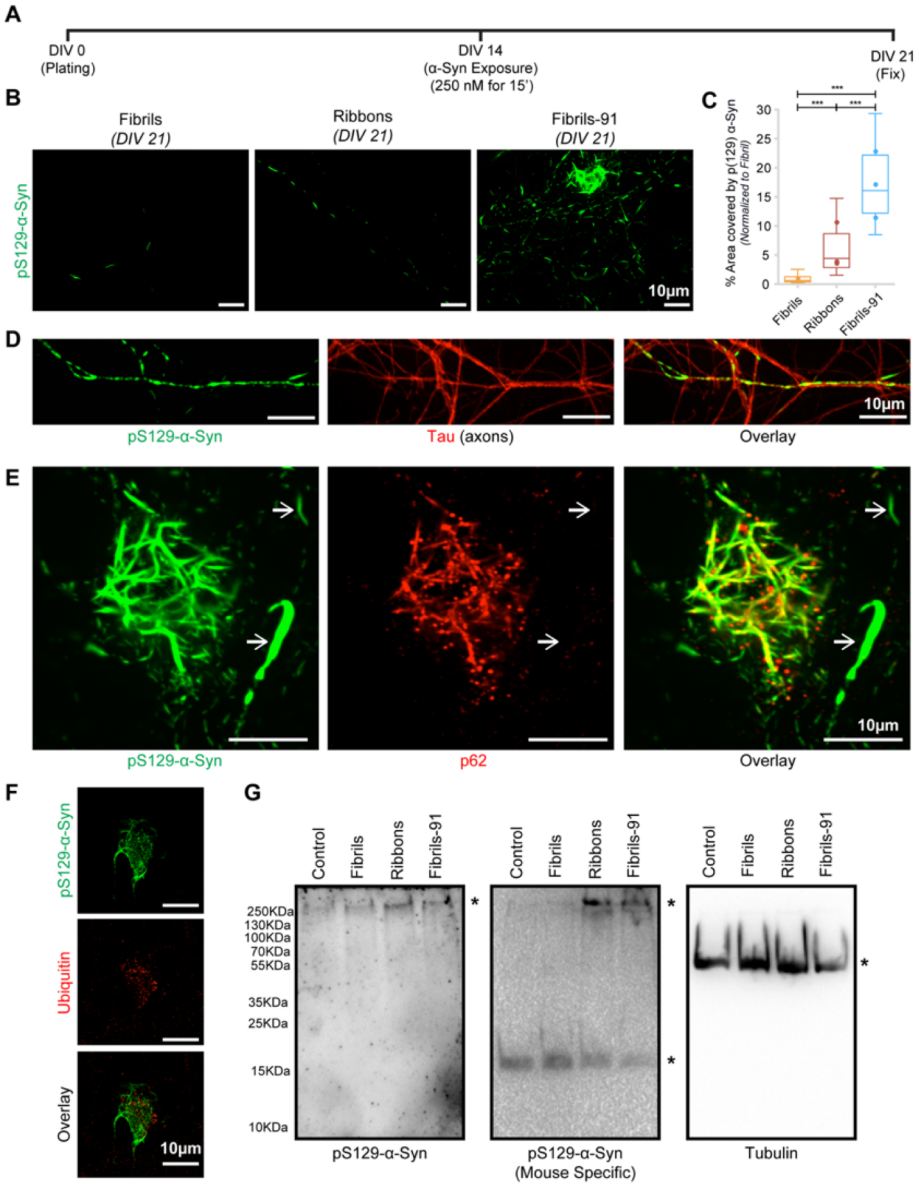
A
DIV 0
(Plating)
DIV 14
(α-Syn Exposure)
(250 nM for 15')
DIV 21
(Fix)
B
Fibrils
(DIV 21)
Ribbons
(DIV 21)
Fibrils-91
(DIV 21)
pS129-α-Syn
10µm
C
% Area covered by p(129) α-Syn
(Normalized to Fibril)
Fibrils
Ribbons
Fibrils-91
D
pS129-α-Syn
Tau (axons)
Overlay
10µm
E
pS129-α-Syn
p62
Overlay
10µm
F
pS129-α-Syn
Ubiquitin
Overlay
10µm
G
Control
Fibrils
Ribbons
Fibrils-91
250KDa
130KDa
100KDa
70KDa
55KDa
35KDa
25KDa
15KDa
10KDa
pS129-α-Syn
pS129-α-Syn
(Mouse Specific)
Tubulin

Figure 6

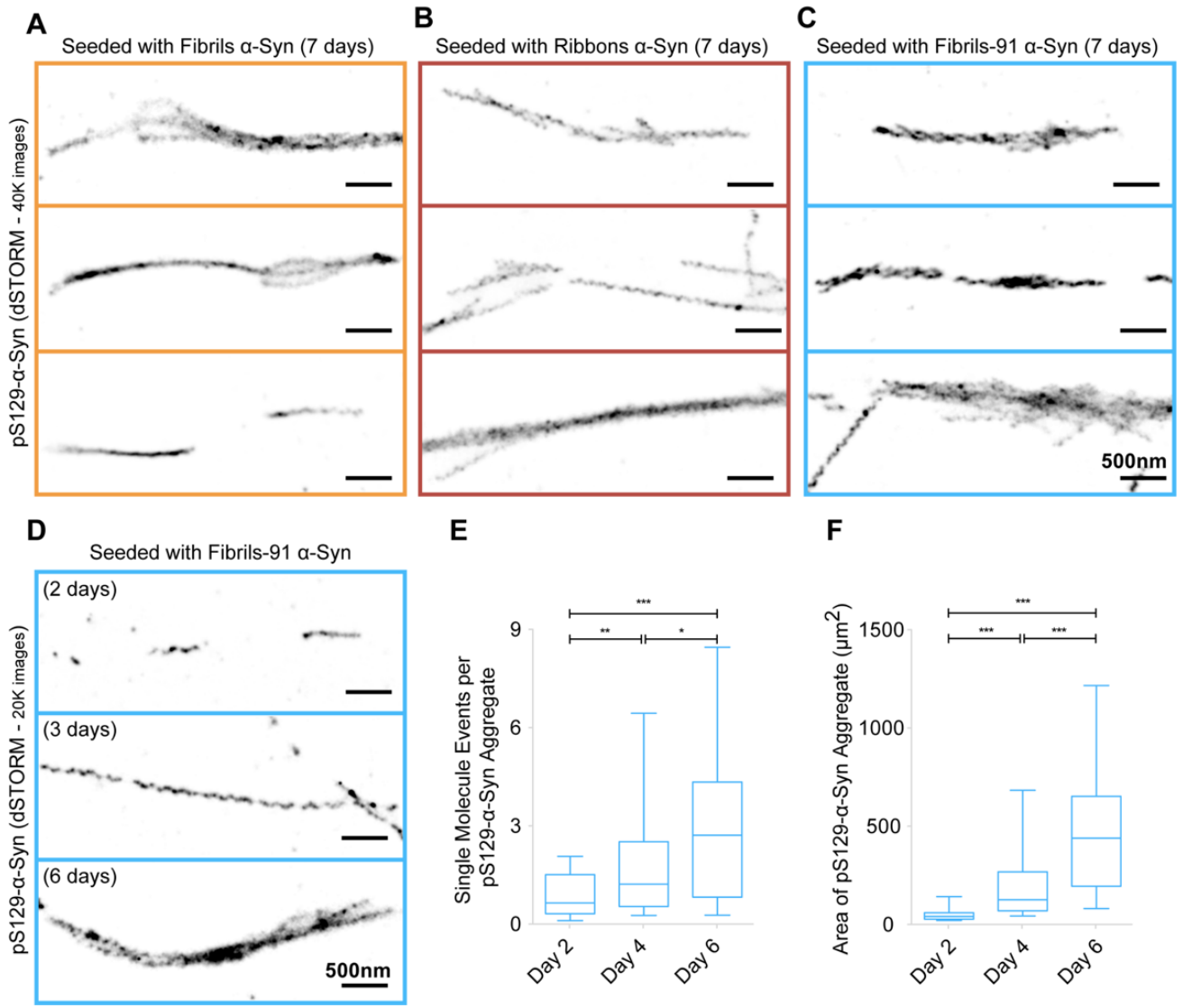
A
Seeded with Fibrils α-Syn (7 days)
B
Seeded with Ribbons α-Syn (7 days)
C
Seeded with Fibrils-91 α-Syn (7 days)
pS129-α-Syn (dSTORM - 40K images)
500nm
D
Seeded with Fibrils-91 α-Syn
(2 days)
(3 days)
(6 days)
pS129-α-Syn (dSTORM - 20K images)
500nm
E
Single Molecule Events per pS129-α-Syn Aggregate
9
6
3
0
***
**
*
Day 2
Day 4
Day 6
F
Area of pS129-α-Syn Aggregate (μm2)
1500
1000
500
0
***
***
***
Day 2
Day 4
Day 6

Figure 7

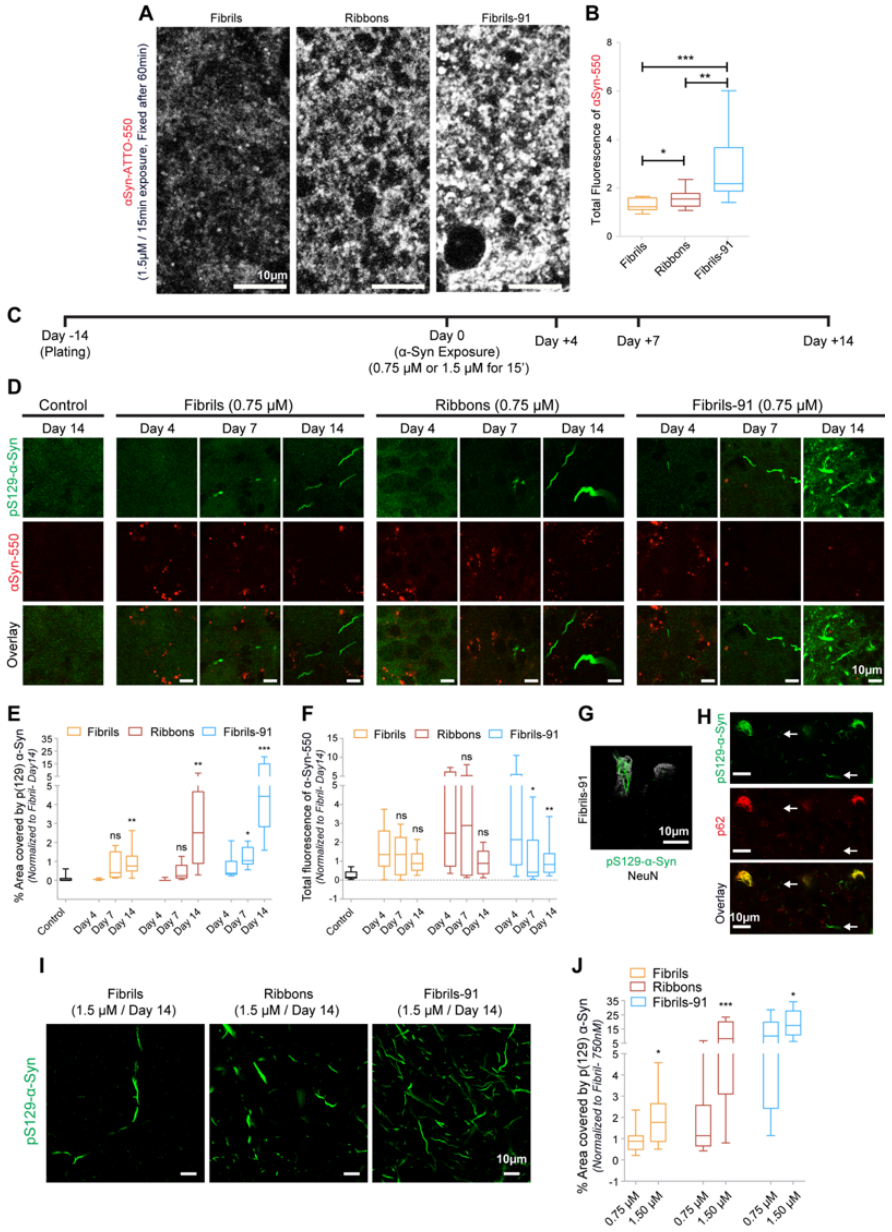
A
Fibrils
Ribbons
Fibrils-91
αSyn-ATTO-550
(1.5μM / 15min exposure, Fixed after 60min)
10μm
B
Total Fluorescence of αSyn-550
Fibrils
Ribbons
Fibrils-91
C
Day -14
(Plating)
Day 0
(α-Syn Exposure)
(0.75 μM or 1.5 μM for 15')
Day +4
Day +7
Day +14
D
Control
Fibrils (0.75 μM)
Ribbons (0.75 μM)
Fibrils-91 (0.75 μM)
Day 14
Day 4
Day 7
Day 14
pS129-α-Syn
αSyn-550
Overlay
10μm
E
Fibrils
Ribbons
Fibrils-91
% Area covered by p(129) α-Syn
(Normalized to Fibril- Day14)
F
Total fluorescence of α-Syn-550
(Normalized to Fibril- Day14)
G
Fibrils-91
10μm
pS129-α-Syn
NeuN
H
pS129-α-Syn
p62
Overlay
10μm
I
Fibrils
(1.5 μM / Day 14)
Ribbons
(1.5 μM / Day 14)
Fibrils-91
(1.5 μM / Day 14)
pS129-α-Syn
10μm
J
Fibrils
Ribbons
Fibrils-91
% Area covered by p(129) α-Syn
(Normalized to Fibril- 750nM)
0.75 μM
1.50 μM

Figure 8

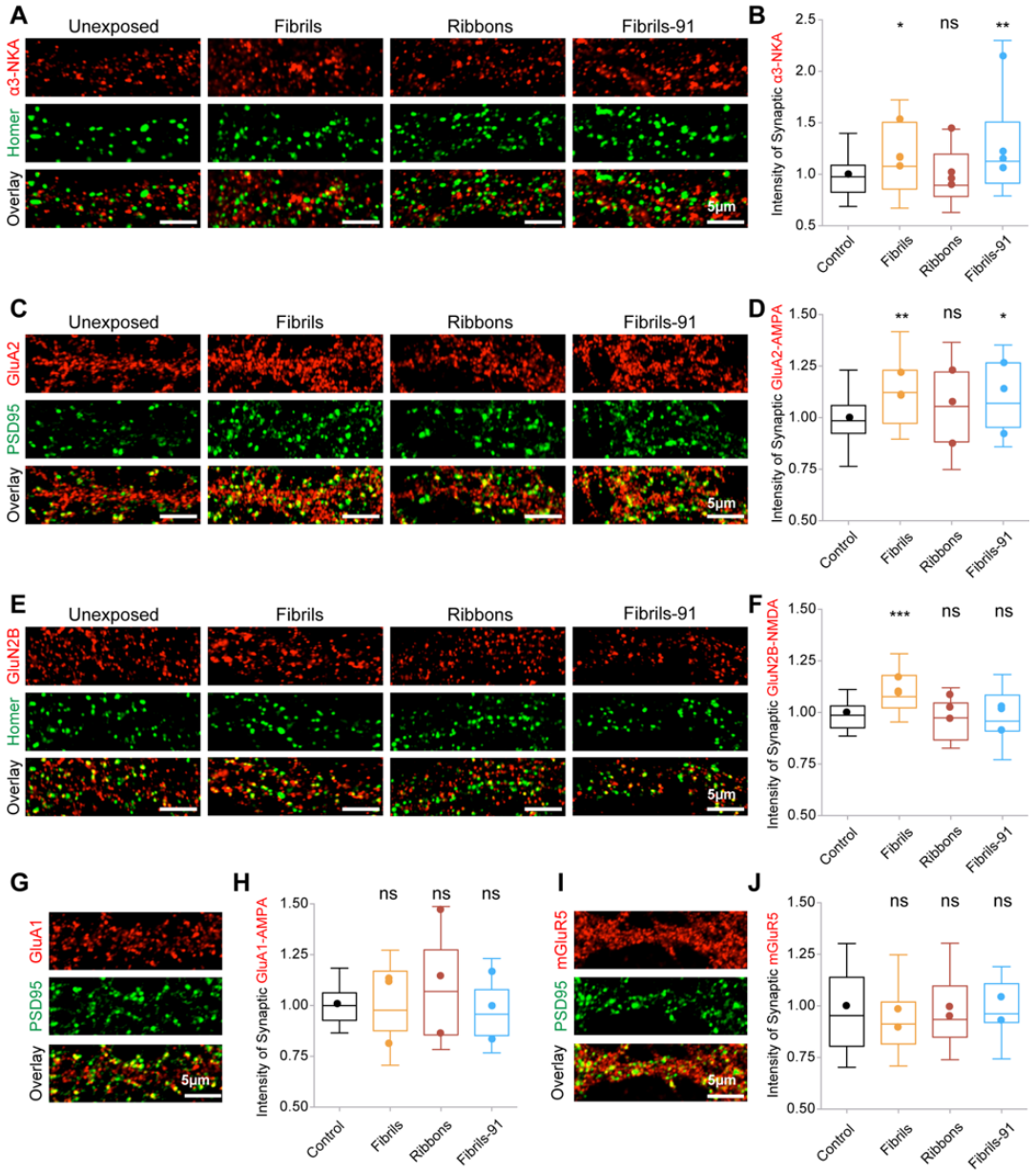
A
Unexposed
Fibrils
Ribbons
Fibrils-91
α3-NKA
Homer
Overlay
5μm
B
Intensity of Synaptic α3-NKA
*
ns
**
Control
Fibrils
Ribbons
Fibrils-91
C
GluA2
PSD95
D
Intensity of Synaptic GluA2-AMPA
**
ns
*
E
GluN2B
F
Intensity of Synaptic GluN2B-NMDA
***
ns
ns
G
GluA1
H
Intensity of Synaptic GluA1-AMPA
I
mGluR5
J
Intensity of Synaptic mGluR5

Figure 9

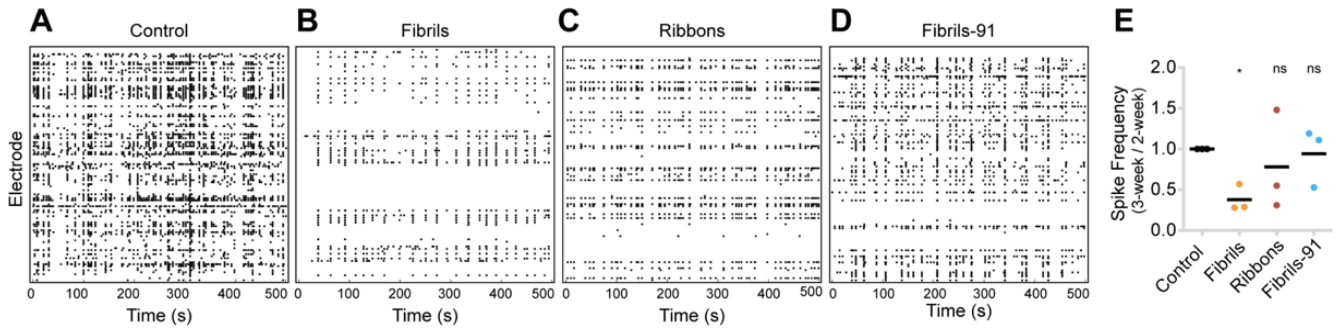
A
Control
B
Fibrils
C
Ribbons
D
Fibrils-91
E
Electrode
0
100
200
300
400
500
Time (s)
Spike Frequency
(3-week / 2-week)
2.0
1.5
1.0
0.5
0.0
*
ns
ns
Control
Fibrils
Ribbons
Fibrils-91